A Thesis for the Degree of
Master of Engineering

Audio Signal Processing using Parametric Array with KZK model

Mano Samuel Andrews

Department of Oceanic Information and System Engineering
GRADUATE SCHOOL
CHEJU NATIONAL UNIVERSITY

2009. 2

Audio Signal Processing using Parametric Array with KZK model

Mano Samuel Andrews

(Supervised by Professor Lee Chong Hyun)

A Thesis submitted in partial fulfillment of the requirement for the

degree of Master of Engineering

2009. 2

Department of Oceanic Information and System Engineering
GRADUATE SCHOOL
CHEJU NATIONAL UNIVERSITY

Audio Signal processing using Parametric Array with KZK model

Mano Samuel Andrews

(Supervised by Professor Lee Chong Hyun)

A Thesis submitted in partial fulfillment of the requirement
for the degree of Master of Engineering

2009. 2

This thesis has been examined and approved.

Jinho Bae

Thesis director, Jinho Bae, Prof. of Oceanic Information and System Engineering

---
Chong Hyun Lee, Prof. of Oceanic Information and System Engineering

---
Dong-Guk Paeng, Prof. of Oceanic Information and System Engineering

5th January 2009

Date

Department of Oceanic Information and System Engineering
GRADUATE SCHOOL
CHEJU NATIONAL UNIVERSITY

SUMMARY

Parametric array for audio applications is analyzed by numerical modeling and analytical approximation. The nonlinear wave equations are used to provide design guidelines for the audio parametric array. A time domain finite difference code that accurately solves the KZK (Khokhlov-Zabolotskaya-Kuznetsov) nonlinear parabolic wave equation is used to predict the response of the parametric array. The time domain code relates the source size and the carrier frequency to the audible signal response including the output level and beamwidth. In considering the implementation issues for audio applications of the parametric array, the emphasis is given to the frequency response and distortion. Specifically we use the time domain code to find out the optimal parameters that will help produce the parametric array with highest achievable output in terms of the average power within the demodulated signal. Parameters such as primary input frequency, audio source radius and the modulation method are given utmost importance. Pre processing techniques to improve the frequency response and to reduce distortion are suggested and demonstrated through the numerical simulation. Eventually the beampattern of the audible signal response is plotted and steered.

TABLE OF CONTENTS

LIST OF FIGURES

CHAPTER I

INTRODUCTION

The parametric array is a nonlinear transduction mechanism that generates narrow, nearly sidelobe free beams of low frequency sound, through the mixing and interaction of high frequency sound waves, effectively overcoming the diffraction limit (a kind of spatial 'uncertainty principle') associated with linear acoustics. Parametric arrays can be formed in water, air, and earth materials/rock [13].

In 1965, H.O. Berktay published the first paper that gave an accurate and more complete theoretical explanation of the parametric acoustic array: Possible Exploitation of Non-Linear Acoustics in Underwater Transmitting applications [4]. However, he claimed that the array would not work in the air. But, Ms. Bennett and Dr.Blackstock went on to prove the existence of parametric array in air and they presented their paper titled: Parametric Array in Air [5]. Though this is a groundbreaking discovery that has opened up new areas of research, it has its limitations. Parametric arrays, while offering high directivity in the low frequency mode, demand a lot of power input which leads to low efficiency levels. High levels of distortion are also of a concern. Therefore here we analyze possible ways to overcome this distortion which in turn translates to improved efficiency. We achieve this by preprocessing the input signal before being transmitted. After obtaining the demodulated output, we use a beamforming and beamsteering algorithm to steer the low frequency, high directivity parametric array in the desired direction.

1.1. Background theory of parametric array:

The non-linearity parameter, B/A, a common term in the field of non-linear acoustics has its origin in the Taylor series expansion [8]. Taylor series expansion of the equation of state $P = P(\rho, s)$, along the isentrope $s = s_0$ yields,

$$p = A\left(\frac{\rho'}{\rho_0}\right) + \frac{B}{2!}\left(\frac{\rho'}{\rho_0}\right)^2 + \frac{B}{3!}\left(\frac{\rho'}{\rho_0}\right)^3 + ..., \tag{1}$$

The significance of B/A in acoustics is the effect of it on the sound speed. Using the relation $c^2 = (\partial P/\partial \rho)_s$, from Eq.1, we obtain,

$$\frac{c^2}{c_0^2} = 1 + \frac{B}{A}\left(\frac{\rho'}{\rho_0}\right) + \frac{C}{2A}\left(\frac{\rho'}{\rho_0}\right)^2 + ..., \tag{2}$$

Taking the square root and performing a binomial expansion yields

$$\frac{c}{c_0} = 1 + \frac{B}{A}\left(\frac{\rho'}{\rho_0}\right) + \frac{1}{4}\left[\frac{C}{2A} - \frac{1}{2}\left(\frac{B}{A}\right)^2\right]\left(\frac{\rho'}{\rho_0}\right)^2 + ..., \tag{3}$$

The parameter B/A thus determines the relative importance of the leading order finite amplitude correction to the small signal sound speed, c_0. For a progressive plane wave, the linear relation $\rho'/\rho_0 = u/c_0$, where u is the particle velocity, maybe substituted into Eq.3 to obtain, $c = c_0 + (B/2A)u$. The above equation can be further written as,

$$dx/dt\big|_u = c_0 + \beta u, \qquad \beta = 1 + B/2A, \tag{4}$$

Thus it can be seen that β, a measure of non-linearity in any given medium through which a wave propagates, is a significant measure of the acoustic non-linearity of the medium. Westervelt presented a theoretical model of the parametric array [1]. The parametric array produces high amplitude ultrasonic waves which demodulate into directional audible sound due to the nonlinear characteristics of the medium through which they travel. As a result, a highly directional beam is produced. One of the main reasons why parametric array is desired is because a parametric array produces a secondary sound beam with similar directivity to that of the primary carrier beam. This is the factor that results in the parametric array producing a low frequency, low beamwidth output.

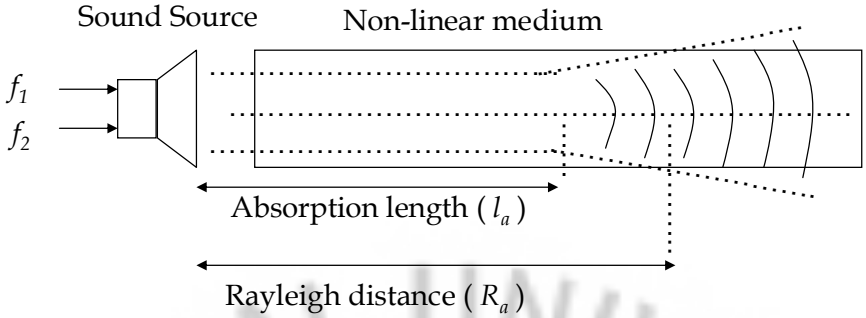

Figure 1 Schematic of the parametric array

An input audio signal of frequency f_1 when amplitude modulated with a frequency f_2 and passed through a medium, the modulated output gets demodulated to produce the difference frequency f_1-f_2, the audio signal, due to the self-demodulation characteristics of the medium through which it is traveling. The self-demodulation of the signal occurs due to the nonlinear characteristics of air [8]. There have been various studies conducted on this self-demodulation process.

For example, if an ultrasonic beam of 45 kHz is modulated with a 500 Hz beam. The demodulated output, the 500 Hz beam will have directivity similar to that of the 48 kHz carrier. The two frequencies are required at the input, the primary and secondary waves, can be represented by the following two equations,

$$p_1(r,z,\tau)=\frac{1}{2j}\left[q_{1a}(r,z)e^{j\omega_a\tau}+q_{1b}(r,z)e^{j\omega_b\tau}\right]+c.c., \tag{5}$$

$$\begin{aligned} p_2(r,z,\tau)=\frac{1}{2j}[&q_{2a}(r,z)e^{j2\omega_a\tau}+q_{2b}(r,z)e^{j2\omega_b\tau} \\ &+q_+(r,z)e^{j\omega_+\tau}]+c.c., \end{aligned} \tag{6}$$

Where,

$$q_1(r,z)=2\pi\int_0^\infty q_1(r',0)G_1(r,z|r',0)r'dr', \tag{7.1}$$

$$q_2(r,z)=\frac{\pi\beta k}{\rho_0 c_0^2}\int_0^z\int_0^\infty q_1^2(r',z')G_2(r,z|r',z')r'dr'dz', \tag{7.2}$$

The above equations describe a sound beam radiated at the two frequencies ω_a and ω_b, which leads to the nonlinear generation of sum and difference frequencies $\omega_\pm=\omega_a\pm\omega_b$ (with

$\omega_a > \omega_b$ assumed) [8]. In addition, harmonics such as $2\omega_a$ and $2\omega_b$ are also generated. The nonlinear interaction is limited to the nearfield of the bifrequency source. It should be noted that farfield and nearfield are not constants but vary based on the frequency used at the input. The Rayleigh distance marks the transition between the nearfield and farfield. The Rayleigh distance is given by,

$$z_0 = \frac{1}{2}ka^2 \tag{8}$$

Now the nonlinear interaction is more or less limited to the nearfield of the bifrequency source. In order to ensure this condition, the condition that needs to be satisfied is $\alpha_0 z_0 \gtrsim 1$, where α_0 and z_0 are attenuation co-efficient and Rayleigh distance, respectively evaluated at the mean primary frequency which is given by,

$$\omega_0 = \frac{1}{2}(\omega_a + \omega_b) \tag{9}$$

Since nearfield is not of any significant importance, we will look further only at farfield and the other parametric characteristics that exhibit themselves here. When the two, finite amplitude, sound waves with different frequencies interact with one another in a medium, secondary waves whose frequencies correspond to the sum and difference of the primary waves are produced as a result of the nonlinearity of the medium through which the waves travel. Based on Lighthill's arbitrary fluid motion equation, Westervelt who observed this phenomenon derived an inhomogeneous equation which is satisfied by the sound pressure of secondary waves,

$$\nabla^2 p_s - \frac{1}{c_0^2}\frac{\partial^2 p_s}{\partial t^2} = -\rho_0 \frac{\partial q}{\partial t}, \qquad q = \frac{\beta}{\rho_0^2 c_0^4}\frac{\partial}{\partial t} p_1^2 \tag{10}$$

Where,

p_s = secondary wave secondary pressure

p_1 = primary wave sound pressure

β = nonlinear fluid parameter, and

c_0 = small signal sound velocity

If a finite amplitude, ultrasound beam, the primary wave f_1, is amplitude modulated by an audio signal $g(t)$ and radiated into the air, the sound pressure p_1 of the primary wave at a distance, x from the array on the axis may be given by,

$$p_1 = p_0 t[1 + mg(t - x/c_0)]e^{-\alpha x} \sin \omega_o (t - x/c_o), \tag{11}$$

Where,

p_o = initial sound pressure of the ultrasound,

m = modulation index, and

α = absorption co-efficient of the carrier sound.

Due to the self demodulation of the signal, a virtual audio signal appears in the far field of the axis. This sound source, the difference frequency, is given by,

$$q = \frac{\beta p_0^2}{\rho_0^2 c_0^4} e^{-2\alpha x} \frac{\partial}{\partial t}\left[mg\left(t - \frac{x}{c_0}\right) + \frac{1}{2} m^2 g^2 \left(t - \frac{x}{c_0}\right)\right]. \tag{12}$$

If the primary sound beam cross section is assumed to be circular with a radius a, then the demodulated audio sound pressure p_s at a point r along the axis is said to be,

$$p_s = \frac{\beta p_0^2 a^2 m}{8\rho_0 c_0^4 \alpha r} \frac{\partial^2}{\partial t^2} g\left(t - \frac{r}{c_0}\right). \tag{13}$$

1.2. Numerical model of Parametric Array:

Although there is no closed form solution to the Khokhlov-Zabolotskaya-Kuznetsov (KZK) equation, to emphasize on the mathematical representation of this parametric array, various mathematical models have been proposed to design the nonlinear characteristics. But one of the most accurate models is the KZK nonlinear wave equation model. The KZK model is known to describe, to the highest degree of accuracy possible, the combined effects of absorption, diffraction and nonlinearity. Here we use the following model to study the characteristics of the parametric audio array.

CHAPTER II

The KZK Model

The KZK nonlinear parabolic wave equation is known to very accurately describe the propagation of a finite amplitude sound beam by combining the effects of absorption, diffraction and nonlinearity. In the derivation of the KZK equation, the sound waves are assumed to form a highly directive beam. Although there are no explicit analytical solutions for the KZK equation, many research groups in pursuit of designing a nonlinear wave propagation model have developed a spectral method, a frequency domain approach or an incomplete time domain model. But, Lee [12] developed a time domain algorithm that solves the KZK nonlinear parabolic wave equation for axisymmetric finite amplitude sound beams. We use this time domain algorithm to model a parametric communication system by transmitting an amplitude modulated signal into the time domain code and receiving the demodulated output at a distance x , in the farfield.

2.1. KZK (Khokhlov-Zabolotskaya-Kuznetsov) Equation:

The KZK (Khokhlov-Zabolotskaya-Kuznetsov) equation is an extension of the Burgers equation. This accounts for the combined effects of nonlinearity, absorption and diffraction.

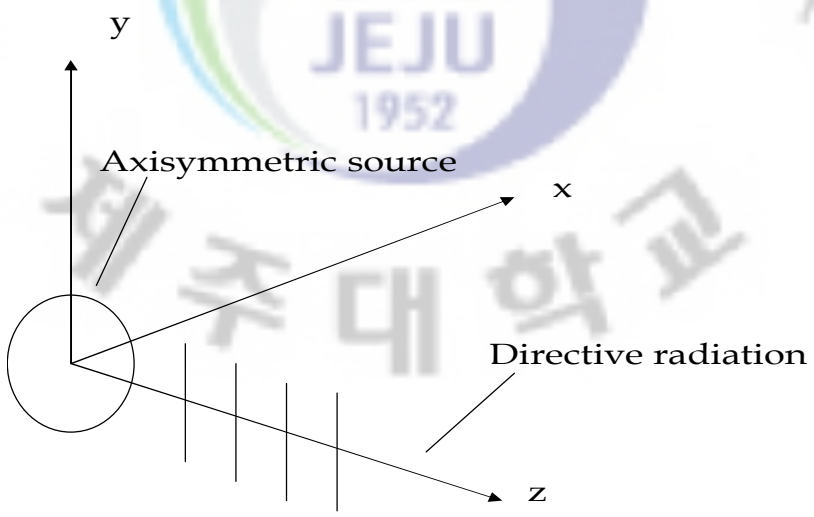

Figure 2 Geometry for radiation from an axisymmetric source

Let **z** be the axis along which the beam propagates and let (**x, y**) be the coordinates perpendicular to the axis. It is known that there is no definite analytical solution to the KZK equation. There with certain assumptions, we use the time domain algorithm here to study and analyze the wave propagation in a nonlinear medium. In regard to the source, certain assumptions that are made are

- It is defined in the plane z = 0,
- It has characteristic radius a,
- It radiates frequencies that satisfy the relation, ka >> 1 and
- The beam emitted by the source is highly directional

Linear theory for directional beams, reveal the existence of near-field and far-field regions. Far-field does not start at a fixed point. The far-field is roughly based on the Rayleigh distance, which is dependent on the carrier frequency involved. The nearfield is characterized by wavefronts that are mostly planar and the far field wavefronts, spherical. This is due to the fact that the waves tend to spread out in the far field as the power of the highly directional beam starts to reduce as it propagates along the *z* axis.

The appropriate scale for the co-ordinates perpendicular to the z axis is less apparent. We impose the stipulation that, like the effects of absorption and nonlinearity, the effect of diffraction must appear at $O\left(\tilde{\varepsilon}^2\right)$ so that all three effects contribute at the same order. In the nearfield, the length scale for variations along the axis of the beam that are caused by diffraction is the Rayleigh distance, which is greater than the length scale *a* across the beam.

The KZK equation is given by,

$$\frac{\partial^2 p}{\partial z\,\partial \tau} - \frac{c_0}{2}\nabla_{\perp}^2 p - \frac{\delta}{2c_0^3}\frac{\partial^3 p}{\partial \tau^3} = \frac{\beta}{2\rho_0 c_0^3}\frac{\partial^2 p^2}{\partial \tau^2}, \tag{14}$$

Where, $\nabla_{\perp}^2 = \partial^2/\partial x^2 + \partial^2/\partial y^2$ is a laplacian that operates in the plane perpendicular to the axis of the beam. In order to improve the computational efficiency in the farfield, a co-ordinate transformation is applied to the KZK equation. This transformation provides the geometry that follows the spherical spreading of the beam in the farfield. The time domain algorithm that we use here solves the KZK equation in a sequence at each range step. First the diffraction term is integrated, then the absorption term and eventually the nonlinear term.

The variable transformations are as follows,

$$\sigma = z/z_o,$$
$$\rho = \frac{r/a}{1+\sigma},$$
$$\tau = \omega_0 t' - \frac{(r/a)^2}{1+\sigma}, \quad (15)$$
$$P = (1+\sigma)\, p/p_0$$

Where,

a = radius of the source,

$\sigma = z/z_0$ is a dimensionless range co-ordinate in terms of Rayleigh distance,

$z_0 = \omega_0 a^2/2c_0$ at the characteristic angular frequency, ω_0

ρ = dimensionless transverse co-ordinate,

τ = dimensionless retarded time,

p_0 = characteristic source pressure amplitude and

p = acoustic pressure.

Thus using the time domain algorithm of the KZK equation, we observe the parametric array's path along the axis of the beam. Now from the KZK equation, Berktay's result, the demodulated secondary frequency pressure, has already been derived as shown in Lee's dissertation. This Berktay's result is given as,

$$p_2(0,z,t') = \frac{\beta p_o^2 a^2}{16\alpha_0 \rho_0 c_0^4 z} \frac{d^2 E^2}{dt'^2} \quad (16)$$

Where,

β = co-efficient of nonlinearity

α_0 = attenuation co-efficient

ρ_0 = density of the propagation medium

z = axial distance from the source

c_0 = speed of sound in air and

E = envelope function.

In order to get the demodulated output, we input the preprocessed modulated data into the KZK equation. The input parameters for the KZK model are given in Table.2.

Now we have a continuous source waveform as the input, the amplitude modulated signal, to the KZK model. For example, let us assume a single tone frequency of 4000 Hz is amplitude modulated with a 20 kHz carrier tone. This amplitude modulated signal will serve as the input to the KZK model. 'DeltaRho' is the transverse step size. The DeltaRho value is normally taken to be 0.03. Rhomax should be in the range of 12> rhomax > 8 as stated by Lee based on experimental results. Here for the KZK model, a value of 10 for Rhomax was chosen. The value of DeltaRho and rhomax remains the same throughout all simulations.

The 'Deltatau' value is based on the formula,

$$\begin{aligned} \Delta\tau &= 2\pi/60, \quad \Gamma < 1, \\ &= 2\pi/120, \, 1 \le \Gamma \le 10, \\ &= 2\pi/240, \, 10 \le \Gamma \le 200. \end{aligned} \tag{17}$$

In our simulations, we settled for a Deltatau value based on the Goldberg number obtained. Since the Goldberg number is dependent on the absorption co-efficient which in turn is dependent on the carrier frequency, the Deltatau value keeps changing based on the input signal considered.

Where, Γ, the Goldberg number is given by, $\Gamma = N/A$ (18)

N = Nonlinearity parameter, $z_0/\tilde{z}$ and

A = Absorption parameter, $\alpha_0 z_0$

In order to observe the propagation of a wave along the axis of the beam, we need to specify 'Sigma 'points or ' watch points'. The distance between each point is determined by the step size. There are two methods based on which the step size is designed. The discontinuity in the source' step function results in numerical oscillations in the nearfield as can be seen in Fig.3. In order to overcome these oscillations, we opt for an Implicit Backward Finite Difference (IBFD) method which is effective in damping the oscillations. The downside to this is the fact that the IBFD method requires small step sizes for accurate results. The step size ($\Delta\sigma$) used here is .001. As mentioned before, smaller step sizes translate into higher computation time.

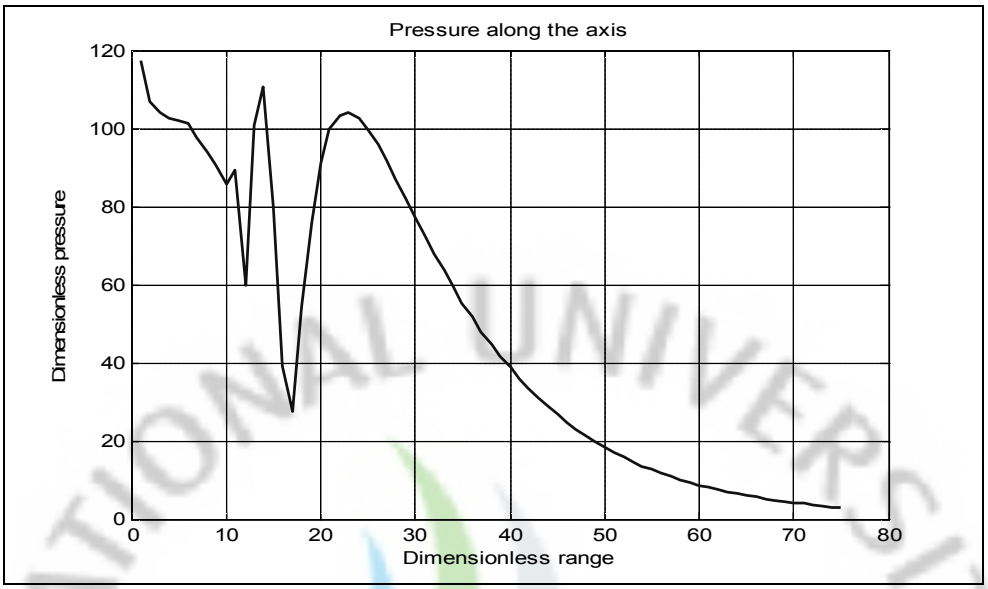

Figure 3 Propagation of a beam along the axis

In order to reduce the computation time, we can opt to use the Crank-Nicolson Finite Difference (CNFD) method beyond the oscillatory region since the CNFD method allows the usage of large step sizes. The step size ($\Delta\sigma$) used here is .0035. With a source radius of d, and a transverse co-ordinate rho, it is possible to determine the radially spreading acoustic wave in the farfield. The transformed pressure P has the spherical spreading factor 1/z factored out.

2.2. Self-Demodulation:

The self-demodulation of the signal is quite an interesting study that has its applications in various fields. Companies such as Holosonics and ATC have been able to exploit this feature to commercialize products that produce high directivity output. Now how does a modulated signal automatically get demodulated? Consider this. The source condition for a piston is given by,

$$p(r,0,t) = p_0 f(t) H(a-r), \qquad f(t) = E(t)\sin\left[\omega_0 t + \phi(t)\right] \tag{19}$$

Where, amplitude modulation *E(t)* and phase modulation $\phi(t)$ are slowly varying functions of time. As already mentioned earlier, we consider the attenuation co-efficient to be large enough ($\alpha_0 z_0 \gtrsim 1$) to contain the non-linear interaction in the nearfield based on the Rayleigh Distance. The instantaneous angular frequency of the carrier wave is $\Omega(t) = \omega_0 + d\phi/dt$. Based on the parametric array model, , the primary beam is considered to be a collimated plane wave, and

further assume that the exponential attenuation acts locally based on the instantaneous angular frequency:

$$p_1(r,z,t) \simeq p_0\, e^{-\alpha(\tau)z}\, E(\tau)\, \sin[\omega_0\tau + \phi(\tau)]\, H(a-r) \tag{20}$$

Now, the frequency content of the secondary pressure, p_2, based on the difference frequency, is determined by, p_1^2 . The high frequency spectrum is absorbed more rapidly than the low frequency spectrum. Therefore most, or all of the output is based on the low frequency spectrum contribution which is given by,

$$p_1^2(r,z,t) \simeq \frac{1}{2} p_0^2\, e^{-\alpha(\tau)z}\, E^2(\tau)\, H(a-r) \tag{21}$$

The length of the non-linear interaction region itself is given by,

$$L_a = (2\alpha_0)^{-1} \tag{22}$$

A further assumption is made that the absorption of the nonlinearly generated low-frequency components is a relatively weak effect, which is justified if E(t) and $\phi(t)$ are slow varying functions of time, corresponding to the very low frequencies. Now the wave equation for p2 thus becomes,

$$\frac{\partial p_2}{\partial z} - \frac{c_0}{2}\int_{-\infty}^{\tau}\left(\nabla_\perp^2 p_2\right)d\tau = \frac{\beta}{2\rho_0 c_0^3}\frac{\partial p_1^2}{\partial \tau}. \tag{23}$$

Using Fourier transforms and the definition of Green's function, one finds that the solution for the demodulated output along the axis of the beam for arbitrary $p_1(r,z,\tau)$ is,

$$p_2(0,z,\tau) = \frac{\beta}{2\rho_0 c_0^4}\frac{\partial^2}{\partial \tau^2}\int_0^z\int_0^\infty p_1^2\left[r', z', \tau - \frac{r'^2}{2c_0(z-z')}\right]\frac{r'\,dr'\,dz'}{z-z'} \tag{24}$$

Substituting Eq.21 into Eq.24 yields,

$$p_2(0,z,\tau) = \frac{\beta p_0^2 a^2}{16\rho_0 c_0^4 z}\frac{\partial^2}{\partial \tau^2}\frac{E^2(\tau)}{\alpha(\tau)}. \tag{25}$$

For ϕ = const and therefore, $\alpha(\tau) = \alpha_0$. Hence the above equation reduces to Berktay's solution, which is, given in Eq.16.

2.3. KZK input parameters:

The KZK model requires an input signal which is modulated with a carrier and passed through the 'air channel'. Although our ultimate aim is to be able to send in an audio input source signal, we begin by using a single tone signal as the input. This single tone signal which is generated is amplitude modulated with a carrier and is sent into the KZK model.

2.3.1. Single tone input signal:

In order to study the parametric array process, we begin with an input source signal as a single tone signal. This single tone signal serves as the input to the parametric array model. For a sampling frequency of 10000 Hz, we generate a single tone signal of 1000 Hz. The single tone signal of 1000 Hz, consisting of 301 samples is shown in both the frequency and time domain,

The single tone signal is amplitude modulated with a carrier of 4 kHz. The sampling frequency is 10 kHz. The modulation index, 'm' used in the modulation scheme here is 0.7. Previous research teams studying the distortion effects in parametric array have shown that varying the modulation index helps control the level of distortion [6]. Low modulation index brings about low levels of distortion and a high level of modulation index brings about high distortion levels. But a low modulation index also means that there is not a significant amount of modulation for the signal to be transmitted as a modulated wave.

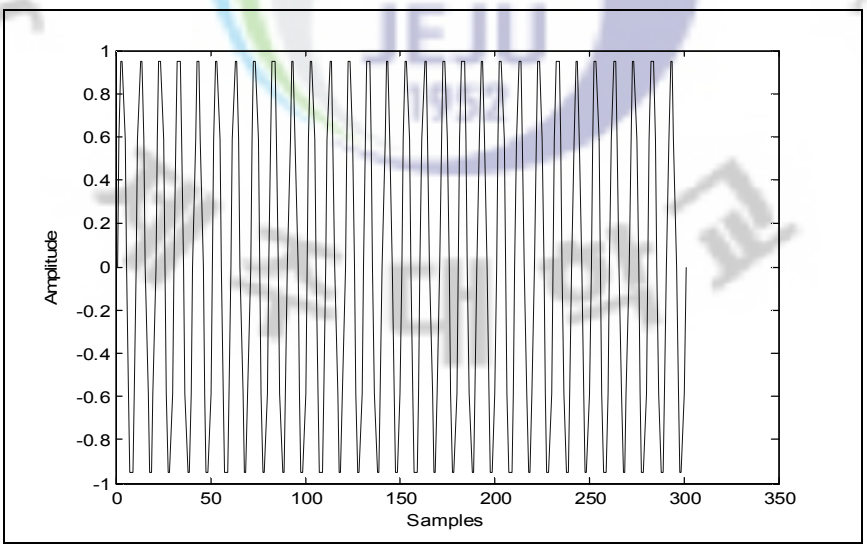

Figure 4 Single tone input signal

The frequency response of the input signal is as follows,

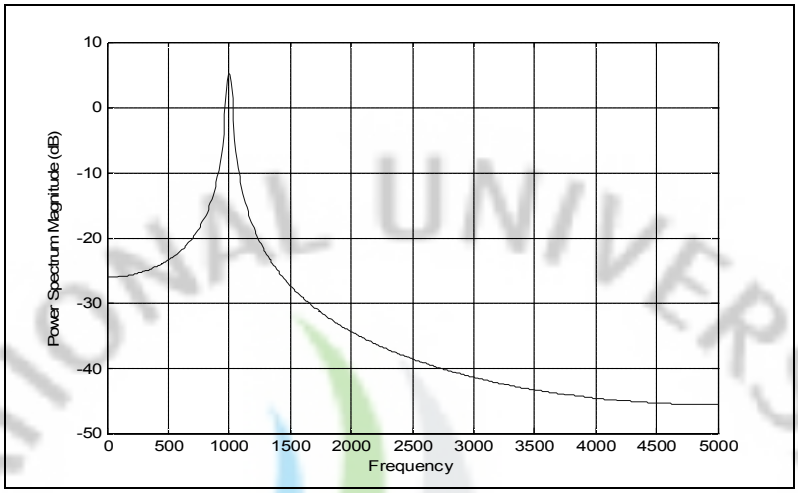

Figure 5 Frequency response of single tone

After amplitude modulation, the modulated signal is passed through a non-linear 'air column'. The demodulated signal is as can be seen in Fig.6.

At a distance of 2.9 meters

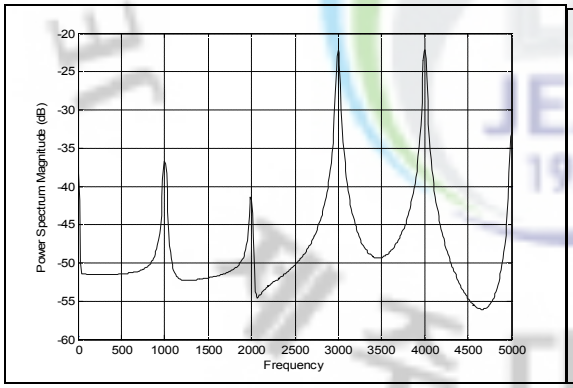

At a distance of 7.4 meters

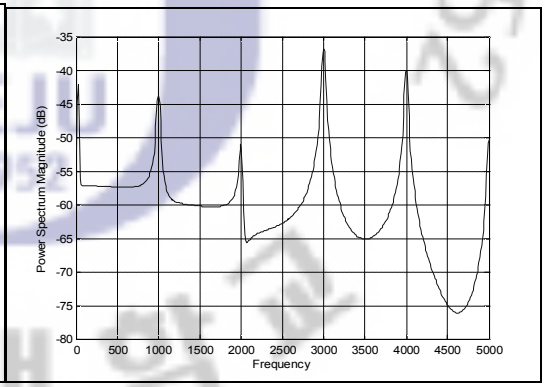

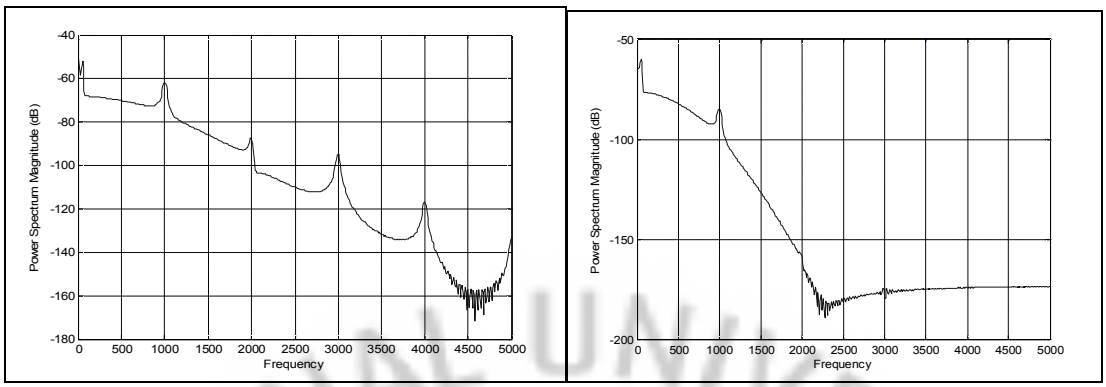

Figure 6 Demodulated signal

At a distance of 32.1 meters At a distance of 86.5 meters

The time domain plot of the output signal can be seen as shown below. At a distance of 1.02 meters, the signal is yet to take shape. But at a distance of 3.4 meters, the demodulated signal appears.

At a distance of 2.9 meters At a distance of 7.4 meters

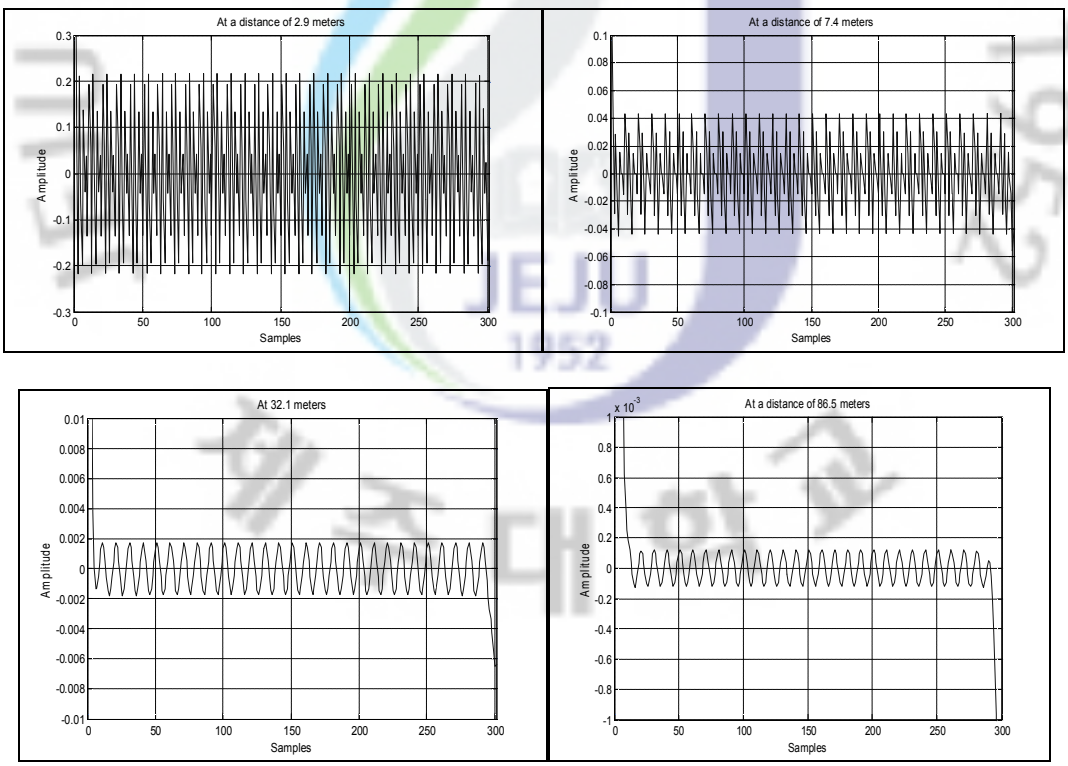

Figure 7 Time domain representation of the demodulated signal

At a distance of 32.1 meters At a distance of 86.5 meters

One of the most important factors that should be brought to the reader's mind is the Rayleigh distance. Now the Rayleigh distance is a rough estimate of where the far field begins. In this single tone frequency input source, with a carrier frequency of 4 kHz, the Rayleigh distance is estimated to be at a distance of 2.47 meters. Therefore from the above plots, it can be seen that the plots shown are relatively in the nearfield and the farfield.

2.3.2. Effect of the change in the number of samples:

Initially we study the effect of changing the number of samples of the input signal. To be able to identify the variation caused, we vary the length of the input signal. We increase the number of samples from 301 to 501 while the other parameters remain the same.

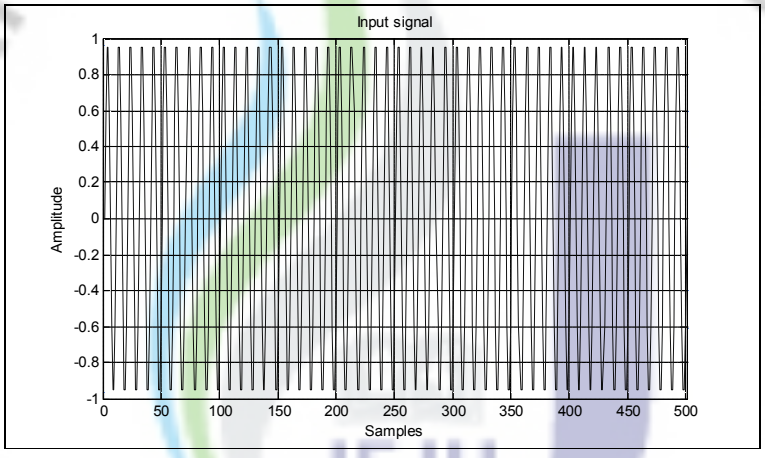

Figure 8 Single tone input signal

As before, the single tone signal is amplitude modulated with a carrier frequency of 40 kHz. The sampling frequency remains at 120 kHz. The modulation index, 'm' used in the modulation scheme here is 0.7.

At a distance of 7.4 meters At a distance of 86.5 meters

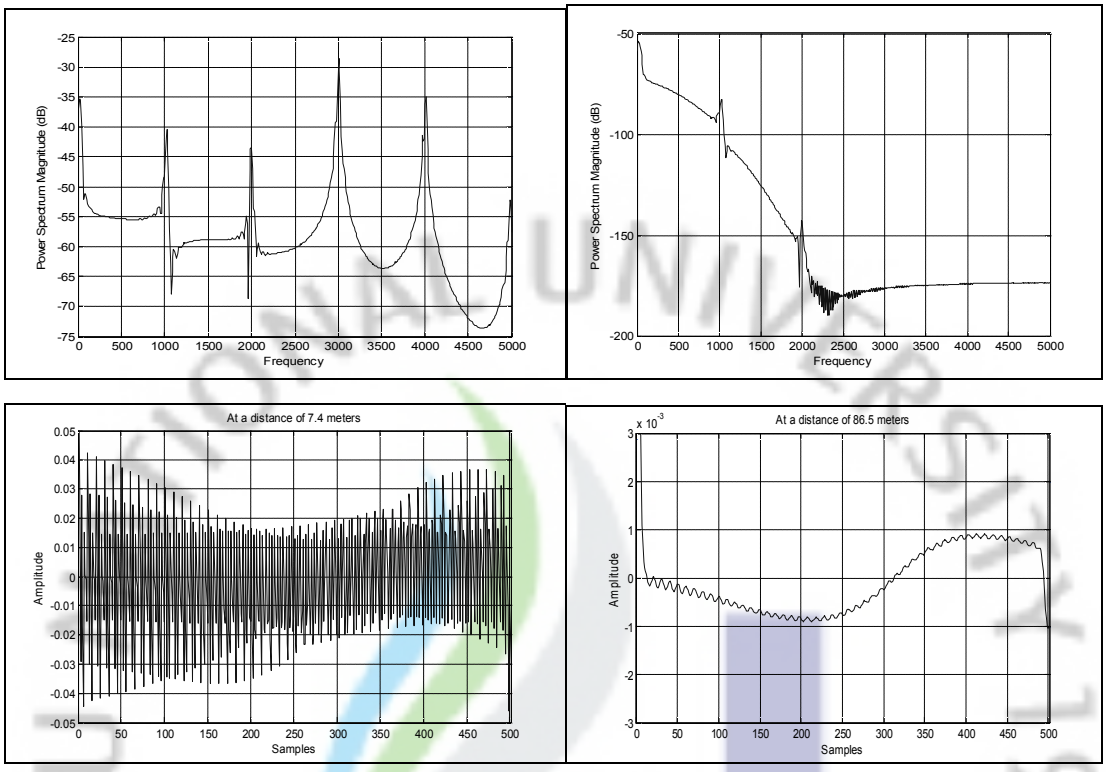

Figure 9 Demodulated data in the frequency and time domain

At a distance of 7.4 meters At a distance of 86.5 meters

After passing the signal through an 'air channel', the demodulated output obtained is as shown in Fig.9. Increasing the number of samples causes the output to change. The reason for the oscillatory behavior of the output signal is due to the low taumax value used in the 'air channel'.

2.3.3. Effect of the change in input source magnitude:

In order to be able to see to what extent the output of the signal is affected if the amplitude of the input signal is altered, we use the single tone signal of 1000 Hz amplified by 10 dB while the other parameters remain the same.

As before, the single tone signal is amplitude modulated with a carrier frequency of 40 kHz. The sampling frequency remains at 120 kHz. The modulation index, 'm' used in the modulation scheme here is 0.7. The increase of 10 dB at the input causes the demodulated signal to have an

increase in its amplitude by 8 dB. Any increase in the amplitude or the magnitude of the input source signal causes the magnitude of the output signal to change as well.

At a distance of 7.4 meters At a distance of 86.5 meters

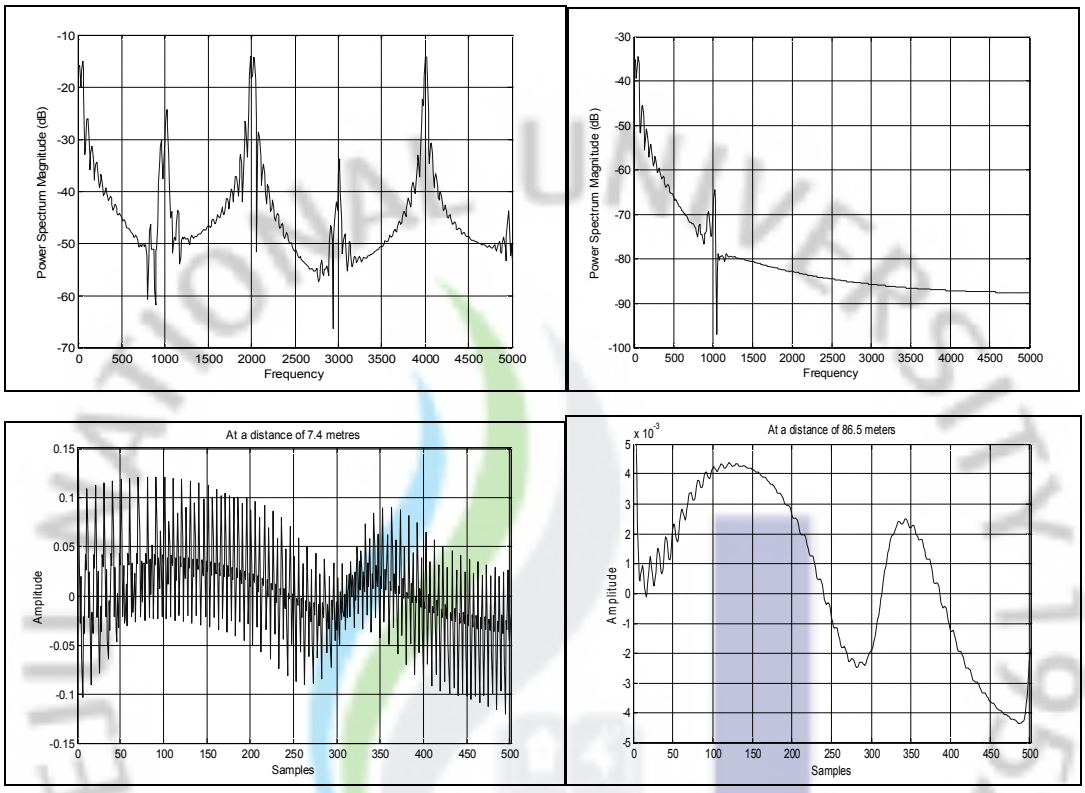

Figure 10 Demodulated data in the frequency and time domain

At a distance of 7.4 meters At a distance of 86.5 meters

Now we compare the different input signals generated due to the different changes made at the input. The demodulated output of a single tone input signal of 1000 Hz and a sampling frequency of 10000 Hz with 301 samples is compared against a single tone input signal of 1000 Hz and a sampling frequency of 10000 Hz with 501 samples. At a distance of 86.5 meters,

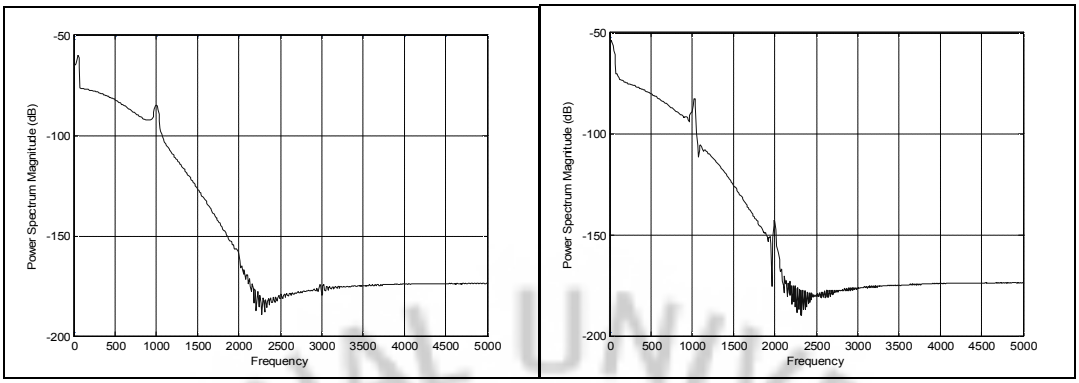

Figure 11 Demodulated output for 301 samples and 501 samples input signal

Thus increasing the number of samples from 301 to 501 does not cause a whole lot of change in the demodulated output. However increasing the number of samples by 200 most definitely helps us achieve a sharper 1000 Hz demodulated signal.

Now we compare the different input signals generated due to the difference in the magnitude of the input signal. The demodulated output of a single tone input signal of 1000 Hz and a sampling frequency of 10000 Hz with 501 samples is compared against a single tone input signal of 1000 Hz and a sampling frequency of 10000 Hz with 501 samples amplified by 10 dB. At a distance of 86.5 meters,

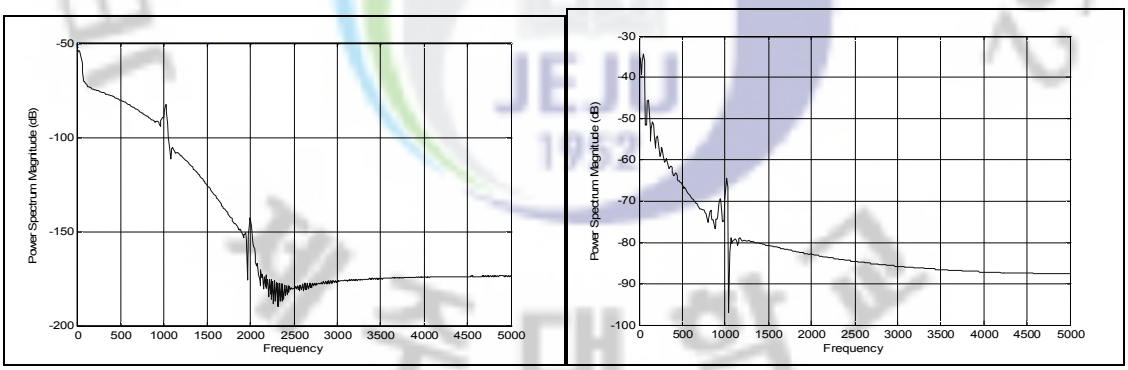

Figure 12 Demodulated signal comparison

Input signal without amplification Input signal with amplification

Thus increasing the magnitude of the input signal causes an increase of the magnitude of the demodulated signal as well.

2.4. Distortion:

One of the biggest shortcomings of the parametric array is the distortion that arises out of the self-demodulation process. As seen in Eq.25, the demodulated signal is proportional to the second time derivative of the square of the modulation envelope. What brings about this distortion is the squaring process within.

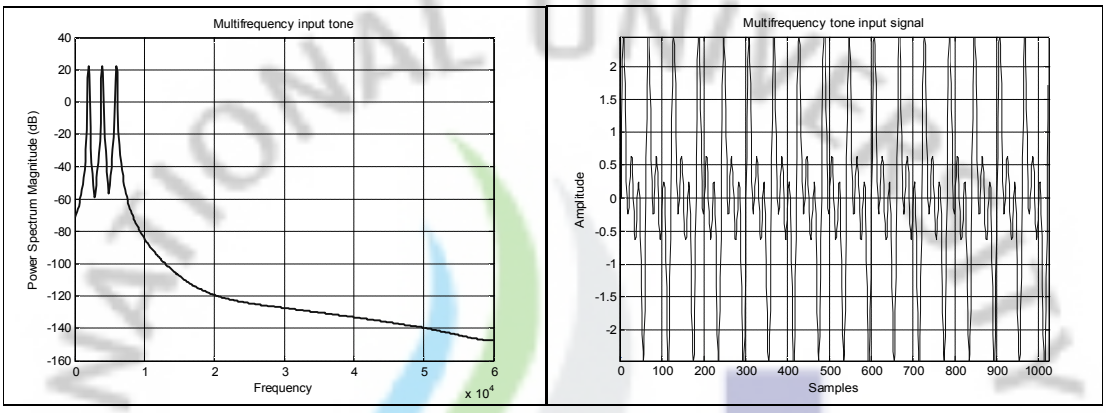

Figure 13 Multi tone audio source signal

The multi tone audio signal in Fig.4 consists of three tones, 2000, 4000 and 6000 Hz signals. Amplitude Modulation of the audio signal of bandwidth 6 kHz with a carrier frequency of 40 kHz (F_c) results in Fig 14. The Amplitude modulation is carried out based on the formula,

$$Y = \{m\ \cos(\omega_m t)\}\ \cos(\omega_c t) \tag{26}$$

Where, m is the modulation index,

ω_m is the signal frequency and

ω_c is the carrier frequency.

From Eq.13, we can say that the squaring process accounts for most of the distortion that arises. In order to overcome this, kite, et al suggested the process of taking a square root of the signal before amplitude modulating the signal with a carrier. This will help overcome distortion that arises due to the harmonics that develop as a result of the signal passing through the channel.

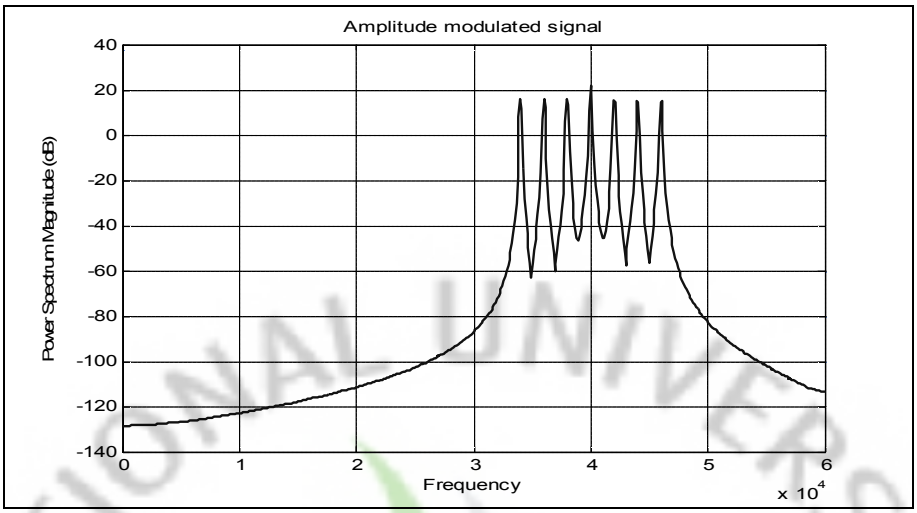

Figure 14 Amplitude modulated multi-tone audio source

The amplitude modulation is performed with a modulation index of 1. The sampling frequency of the multi tone source and the carrier signal is 120 kHz. In order to highlight the effects of distortion, consider the square root process of the multifrequency tone seen in Fig.15. As a result of square rooting the signal, multiple harmonics arise. These multiple harmonics spread from an initial 6 kHz bandwidth to a bandwidth greater than 60 kHz.

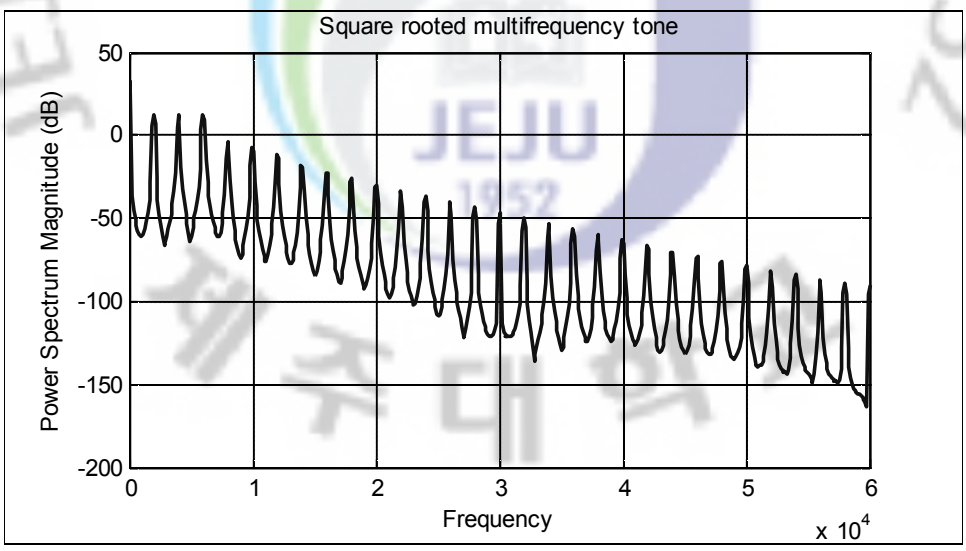

Figure 15 Square rooted multi-tone frequency signal

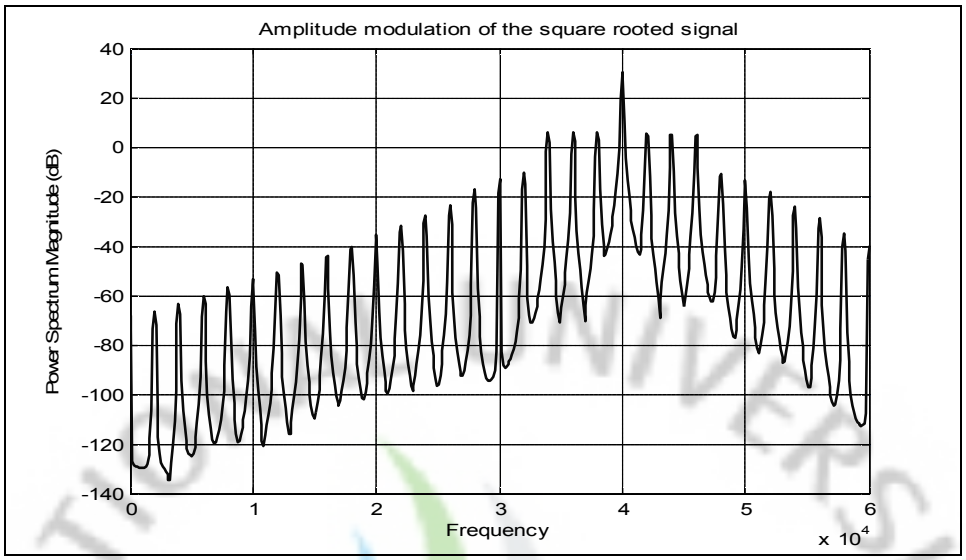

Figure 16 Amplitude modulated square rooted signal

Since the channel is more or less a squaring function, a square root is imposed on a signal that is passed through an air channel to overcome the distortion [6]. These harmonics play a counter effect to the squaring process within the 'air channel'.

Amplitude Modulation of a square rooted audio signal of bandwidth 6 kHz with a carrier frequency 40 kHz (F_c), with a modulation index of 0.7 results in Fig.16. The bandwidth of the modulated signal effectively lies in the range, 30 – 50 kHz for a normal audio signal. But as a result of the square root process, now the bandwidth spans for a wider bandwidth. If this signal, as shown in Fig.16, is passed through the air channel, it will lead to heavy distortion because of the fact that we have n number of harmonics that lie in the audible range. Therefore care should be taken that before the modulated signal is passed into the air column, we get rid of the audible components as depicted in Fig.17. The frequency components that lie in the audible range can be removed by passing the modulated signal through a high pass filter before transmitting it through the air column.

Transmitting signal without passing it through a high pass filter before transmission could result in excessive harmonics which translates into distortion. This characteristic which is more evident with an 'actual' audio signal will be shown later.

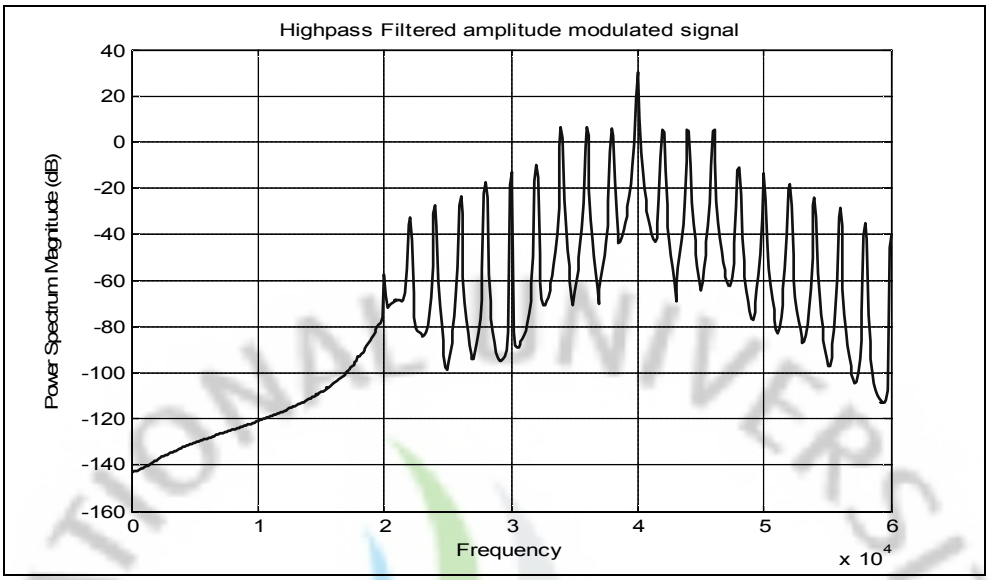

Figure 17 High pass filtered AM signal

2.5. Demodulation due to nonlinearity:

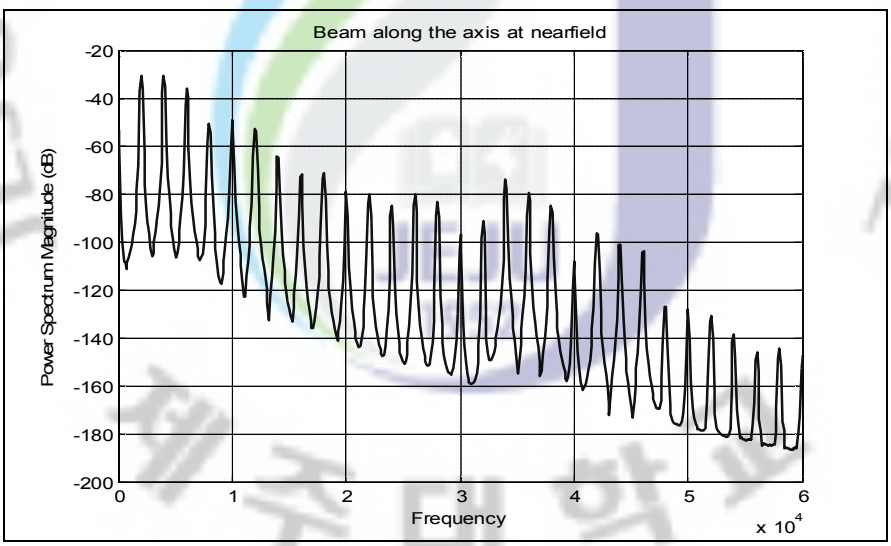

Figure 18 Beam along the axis in the nearfield

Eventually when a high pass filtered modulated signal, as shown in Fig.17 is passed through air, through the process of self-demodulation, the transmitted signal is obtained at a distance, 0.2 meters, at the nearfield, as shown in Fig.18. The Rayleigh distance, with an audio source of radius .15 meter marks the transition from nearfield to farfield, at 8.5 meters.

At a distance of 3.4 meters, at nearfield,

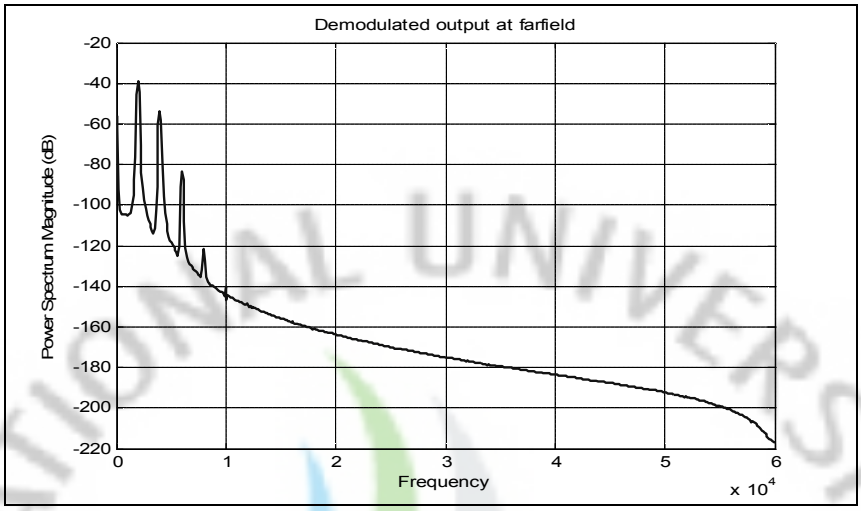

Figure 19 Demodulated signal

At a distance of 15.1 meters, with an amplified demodulated output,

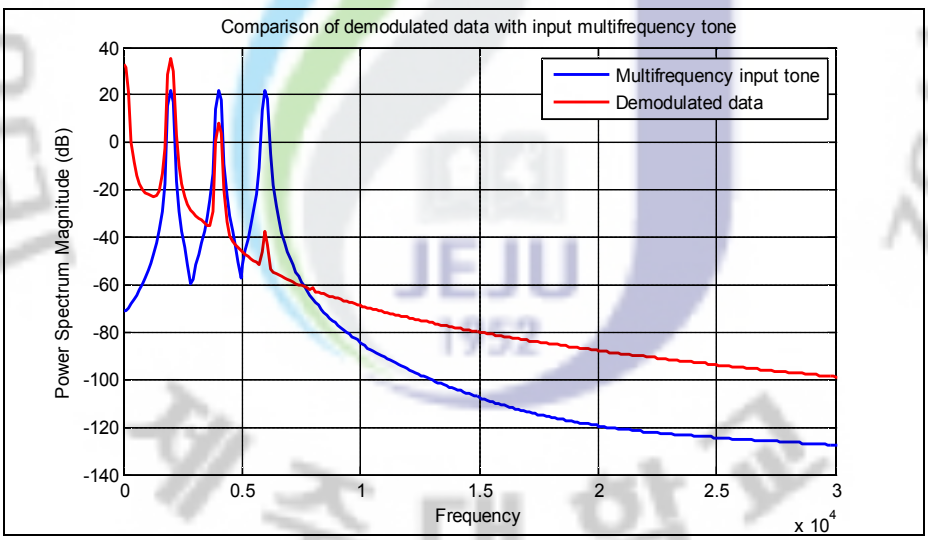

Figure 20 Amplified demodulated output

Comparing the frequency spectrum of original signal with the demodulated signal, we can observe that there exists a certain level of distortion. In case of pure-tone modulation with, $g(t)=\sin \omega t$, the sound pressures from both the signal secondary wave and the second harmonic distortion signal are given by,

$$p_s(t) = -\left(\beta p_0^2 a^2 m\omega^2 / 8\rho_0 c_0^4 \alpha r\right) \sin \omega\left(t - r/c_0\right), \tag{27}$$

$$p_d(t) = -\left(\beta p_0^2 a^2 m^2 \omega^2 / 8\rho_0 c_0^4 \alpha r\right)\cos 2\omega\left(t - r/c_0\right). \quad (28)$$

From the above equations, the second harmonic distortion is given by,

$$\in = \left[\left|p_d(t)\right| / \left|p_s(t)\right|\right] \times 100 = m \times 100\ \% \quad (29)$$

The second harmonic distortion is proportional to the modulation index, m. Therefore while reducing the modulation index certainly reduces the distortion level, it also reduces the amount of modulation between the audio signal and the carrier frequency. Hence reducing the modulation index is not an optimal method to overcome distortion. Since we use an audio signal as the input, we need to reduce the distortion since the modulated signal passing through the medium produces *n* number of harmonics.

2.6. Demodulated data at different ranges:

Based on the input parameters specified above, the demodulated signal at ranges of 0.8, 2.5, 6.8 and 4.2 meters are shown below in a clockwise order.

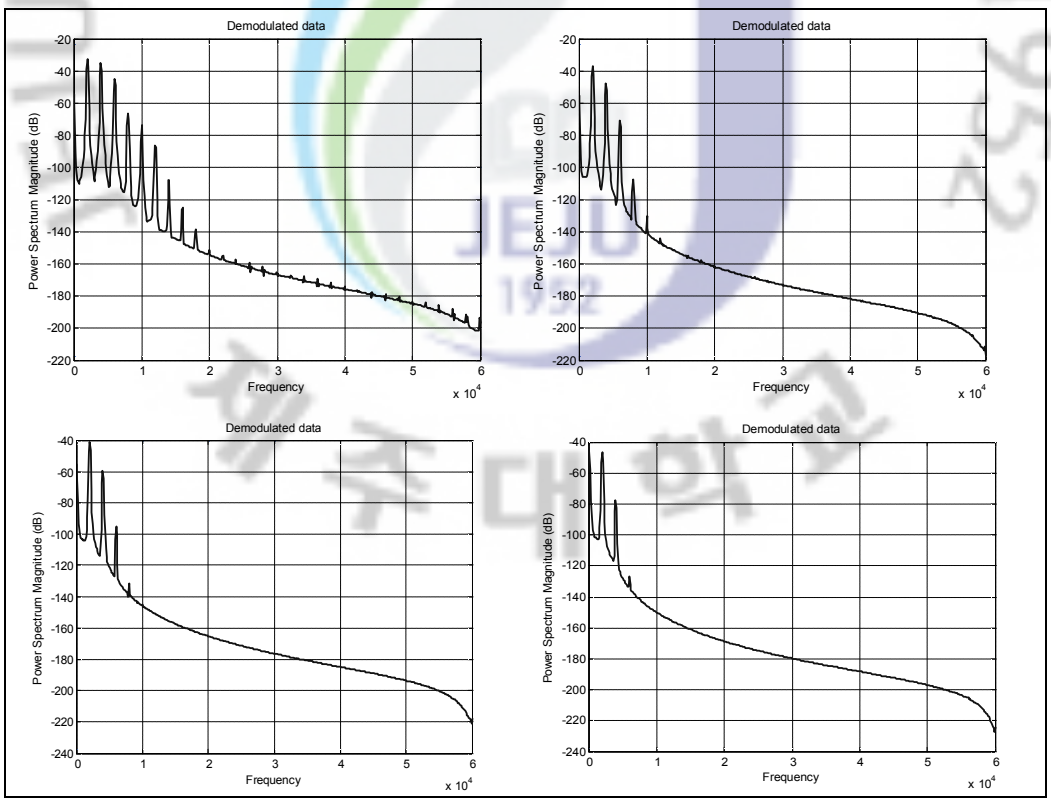

Figure 21 Demodulated multifrequency tone signal

In this single tone frequency input source, with a carrier frequency of 40 kHz, and an input source of diameter 15 cm, the Rayleigh distance is estimated to be at a distance of 8.5 meters. But from the above plots, it can be seen that all the plots shown are relatively in the nearfield. At a distance of 6.8 meters, it was observed that the amplitude of the 8 kHz tone signal was far too negligible. The demodulated signal, in the time domain can be seen at various distances of 0.8, 2.5, 4.2 and 6.8 meters in Fig.22.

At a distance of 0.8 meters

At a distance of 2.5 meters

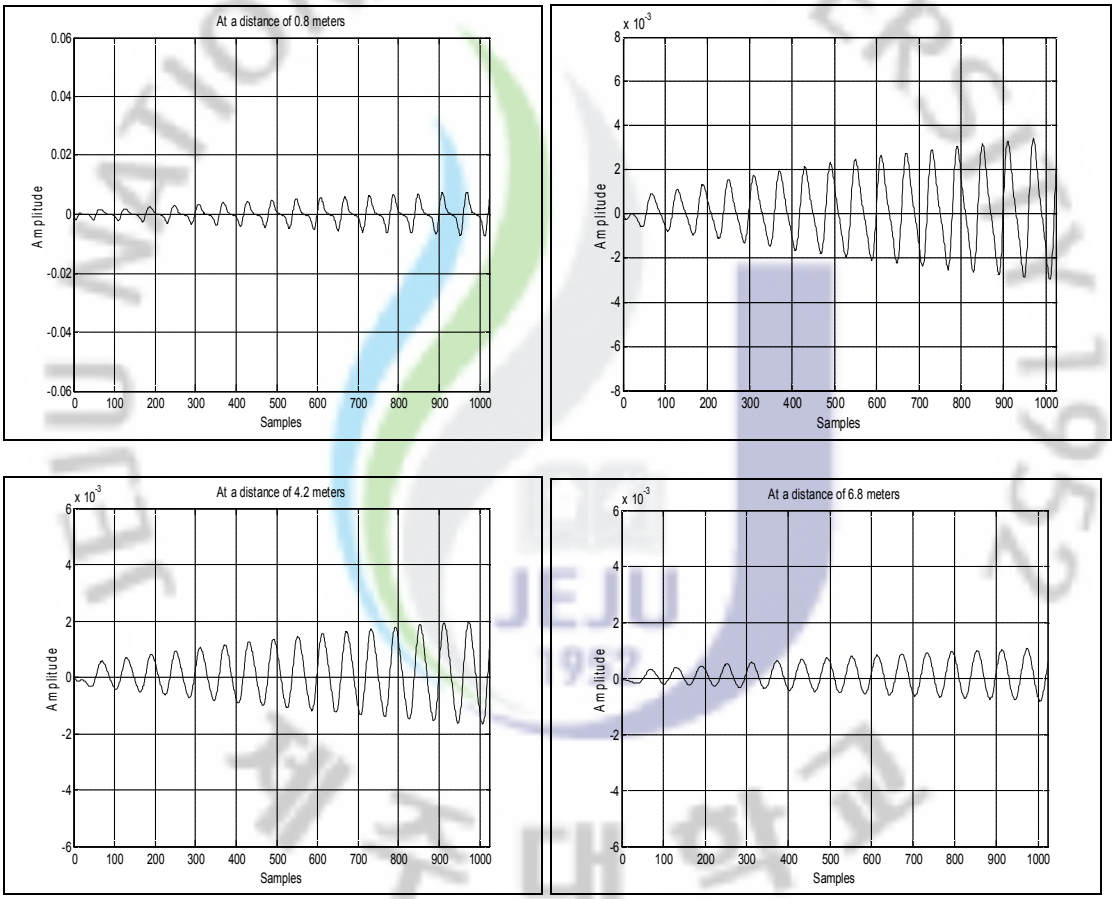

Figure 22 Time domain representation of the demodulated signal

At a distance of 4.2 meters

At a distance of 6.8 meters

CHAPTER III

EFFECT OF THE TRANSDUCER DIAMETER

3.1. Transducer diameter:

Through the square root process of a multi-tone frequency input source before modulation, we were able to establish the fact that it helps overcome distortion. But there are other parameters of critical importance such as the diameter of a transducer and the primary input primary frequency that also help in the process of reducing distortion and increasing secondary frequency pressure levels.

The Rayleigh distance determines the length of the nearfield of a piston, after which the plane-wave like propagation starts to spread. The absorption length of the parametric array determines the region of the virtual array where the nonlinear interaction is occurring. A combination of these two parameters determines the range and the directional behavior of the main and the difference beams. For Berktay's solution to be valid, the Rayleigh distance should be longer than the absorption length. The absorption length is given by,

$$l_a = \frac{1}{\alpha} \tag{30}$$

Where, α is the absorption co-efficient and the Rayleigh Distance is given by Eq.8.

Diameter of size 7 cm:

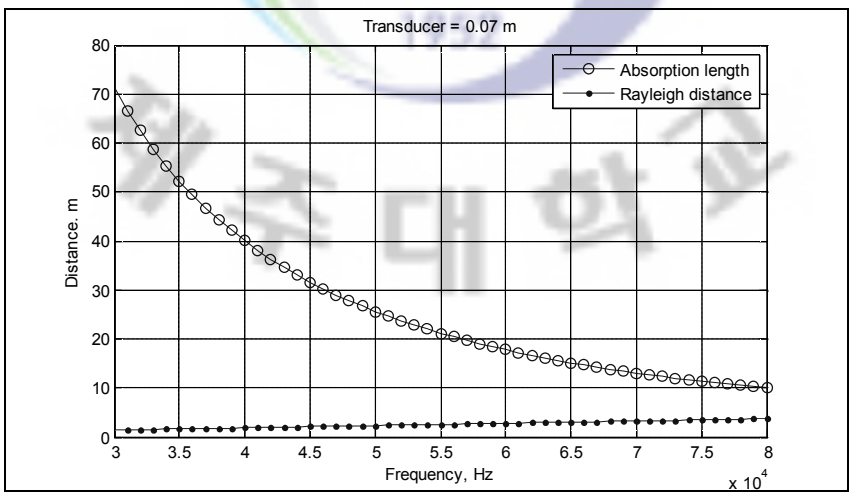

Figure 23 Transducer of radius 7 cm

In order to see the best possible input parameters for a parametric array setup, let us look at a few conditions to find out the desirable parameters. For the above plot, a transducer of radius 7 cm was assumed. The value of the absorption co-efficient varies based on the frequency value. Considering a transducer of radius 7 cm, we see that for frequencies as high as 80 kHz, the Berktay's solution is not satisfied. The absorption length still remains greater than the Rayleigh distance. Therefore a transducer of radius 7 cm is not ideal for primary frequencies that range from 30-80 kHz.

Diameter of size 15 cm:

Using a transducer of radius 15 cm results in the Berktay's condition being satisfied at a primary frequency value of 70 kHz. So if a transducer of this size is used, primary frequencies

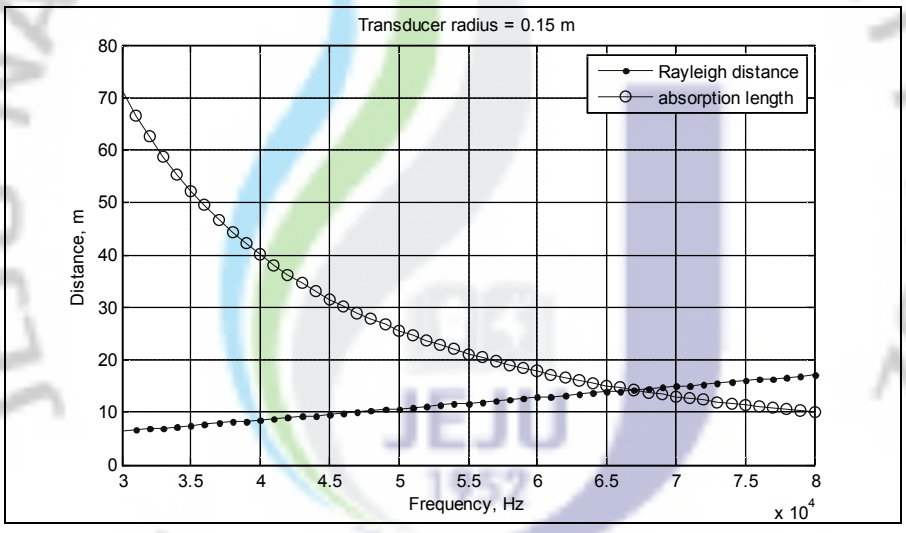

Figure 24 Transducer of radius 15 cm

have to be greater than 70 kHz inorder to get a desirable demodulated signal at the farfield.

Diameter of size 30 cm:

With a transducer of radius 30 cm, the Berktay's condition is satisfied for frequencies beyond 44 kHz. Beyond the 44 kHz range, the absorption length is shorter than the Rayleigh distance which means the demodulated output obtained at this point is favorable for accurate results.

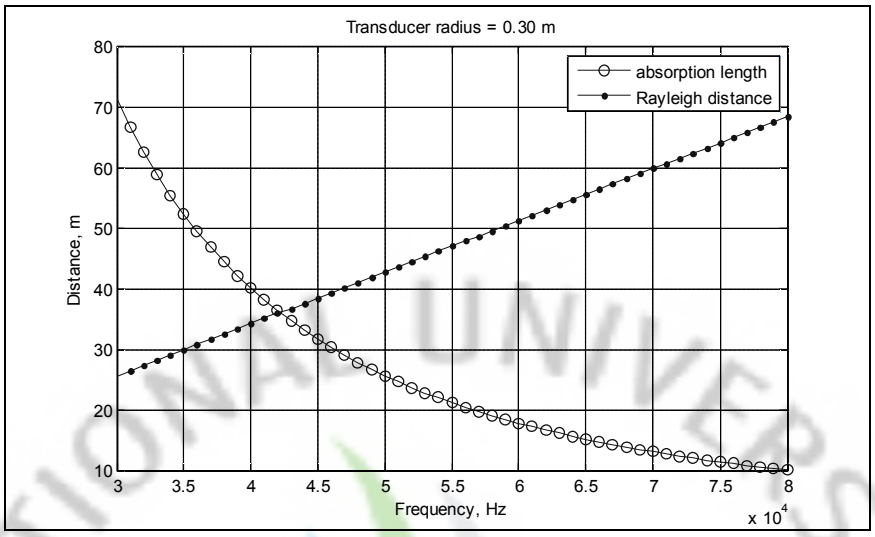

Figure 25 Transducer of radius 30 cm

Relation of Goldberg Number with Radius of transducer:

Higher input pressure, higher the output pressure is the general notion. However, this relation is only valid within the quasilinear assumptions where the nonlinearity is relatively weak ($\Gamma<1$). The Goldberg number Γ is given by Eq.18. Since Γ is proportional to input pressure, high input pressure does not necessarily mean high output pressure. High input pressure results in a higher non-linear parameter. High non-linearity causes saturation of the output response and high distortion.

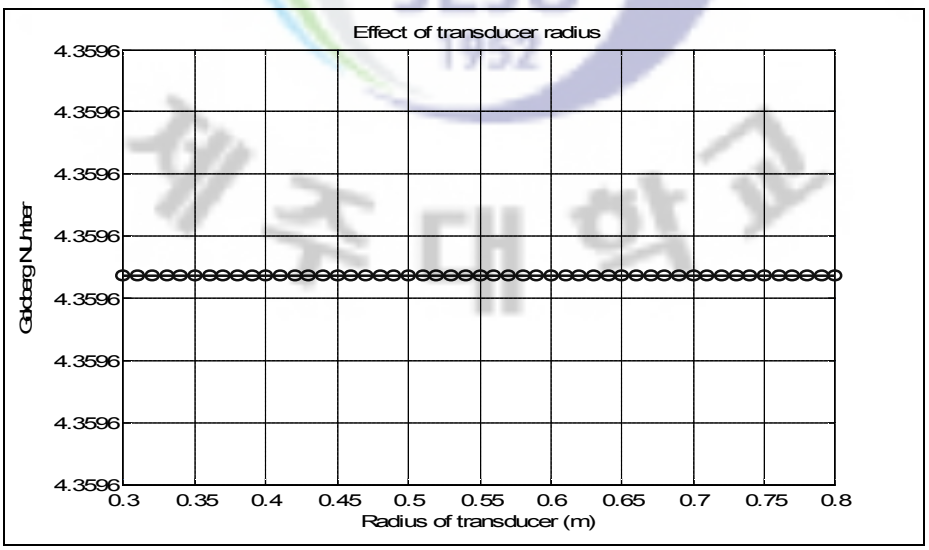

Figure 26 Effect of transducer radius

However the Goldberg number, Γ, depicted on the Y-axis of Fig.26, is independent of the radius of the piston, which is on the X-axis. Therefore the best possible way to increase the output pressure without having to worry about saturation is to increase the size of the piston.

Therefore based on the above results, larger sized transducers seem ideal. But in practical applications, it is not always an ideal option. Therefore in the following portion, we simulate various conditions to estimate the ideal input parameters for an audio source and plot the results.

CHAPTER IV

AUDIO INPUT SOURCE

4.1. Effect of the sampling frequency:

Now, let us consider an audio file (.wav file) as the input source instead of a multi-tone frequency signal. The input audio signal, whose frequency response can be seen in Fig.27, with a total of '39922' samples has a sample frequency of 8 kHz. The audio file reads "The discrete Fourier transform of a re-evalued signal is conjugated symmetric". The sampling frequency of 8 kHz means the highest frequency component f_{max} is of 4 kHz. The objective is to send amplitude modulated waveform into the KZK model and observe the demodulated output at a particular distance [2].

The audio file with an f_{max} of 4 kHz if modulated with a carrier of 5 kHz would result in an output signal with a spectrum of 9 kHz. However the 9 kHz is not in the ultrasonic range and remains audible. If this audible modulated signal is passed into the air channel, it will lead to more audible harmonics which translates into distortion. Therefore, we have to upsample the message to a higher rate.

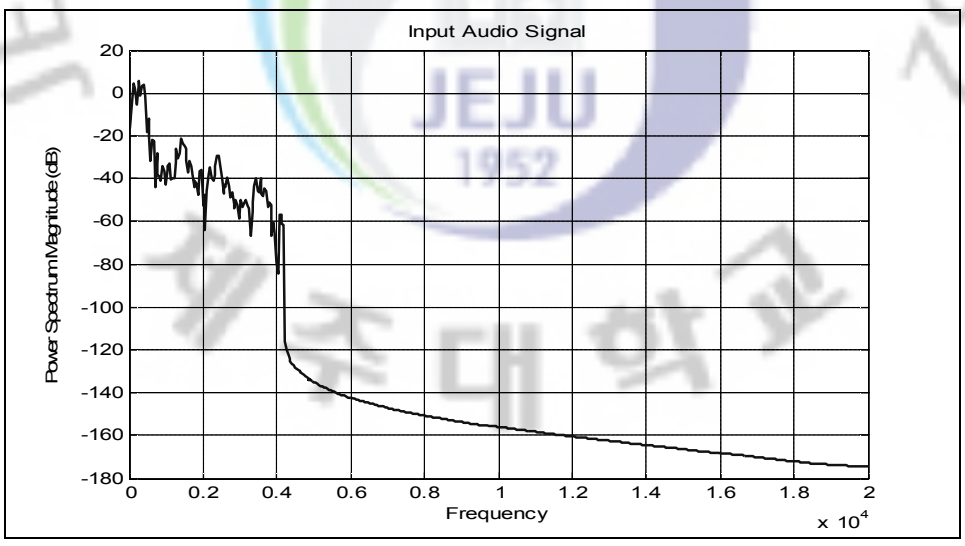

Figure 27 Input Audio Signal

The range of acceptable carrier frequencies is constrained by the message bandwidth. The original message must be upsampled by an integer factor U to ensure that there is no aliasing. To

avoid aliasing near DC, we need the carrier frequency $f_{CARRIER}$ to be greater than $f_{MSG,MAX}$. The highest frequency possible in a SSB or DSB signal is then $f_{MOD\,MAX} = f_{CARRIER} + f_{MSG\,MAX}$. Since the simulations must be carried out digitally, this implies that the overall sampling rate, $f_{OVERALL}$, must be greater than $2f_{MOD\,MAX}$.

Now we increase the sampling frequency to 40 kHz. With a carrier frequency, Fc of 15.9 kHz and a sampling frequency of 40 kHz, the audio signal is square rooted to compensate for distortion and amplitude modulated.

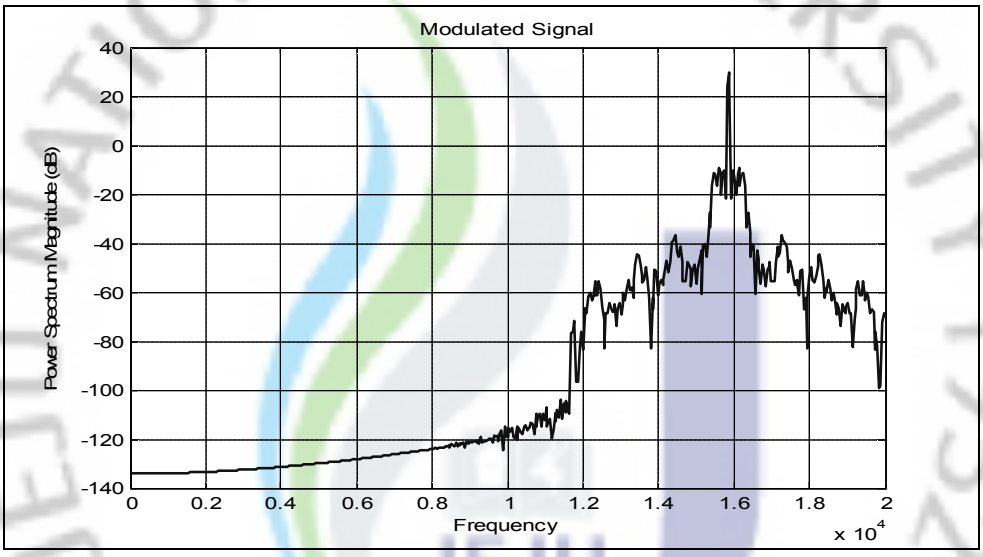

Figure 28 Amplitude modulated signal

The amplitude modulated signal is passed into the channel, the KZK model. The KZK model will be explained in a subsequent chapter.

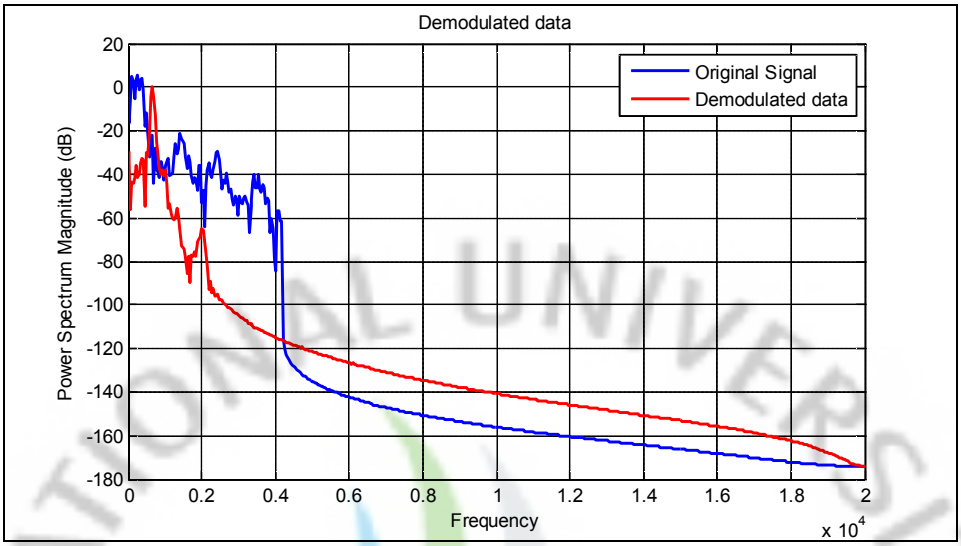

Figure 29 Comparison of demodulated data with input signal

With a source radius of .15 meters, the Rayleigh distance determines that farfield starts approximately at a distance of 3.20 meters. The amplitude modulation was done with a modulation index of 0.7. This modulated signal passed through air, due to the inherent nonlinear properties of air, automatically demodulates and produces the audio output at a certain distance, of 3.7 meters, at the farfield.

From Fig.28, it is plain obvious to see that there exists certain frequency components in the audible range. If there exists frequency components in the audible range, passing this signal through the channel will only generate more harmonics which will lead to a greater level of distortion. In Fig.29 it can be seen that as the demodulated data takes shape, it varies more from the original audio file as evident in the plot. Therefore, we need to choose a higher carrier frequency.

To begin with, we need to increase the sampling frequency of the audio signal in order to reduce distortion. Therefore the audio signal was upsampled by an integer factor, U of 10. After upsampling, the audio signal has a sampling frequency f_s of 80 kHz as can be seen in Fig.30.

This audio signal is then amplitude modulated with a carrier signal of 35.9 kHz. The amplitude modulated signal does not have a frequency component in the audible range as evident

in Fig.31. For a source radius considered to be of 0.15 meters, the farfield distance is determined to begin at a distance of 7.6 meters.

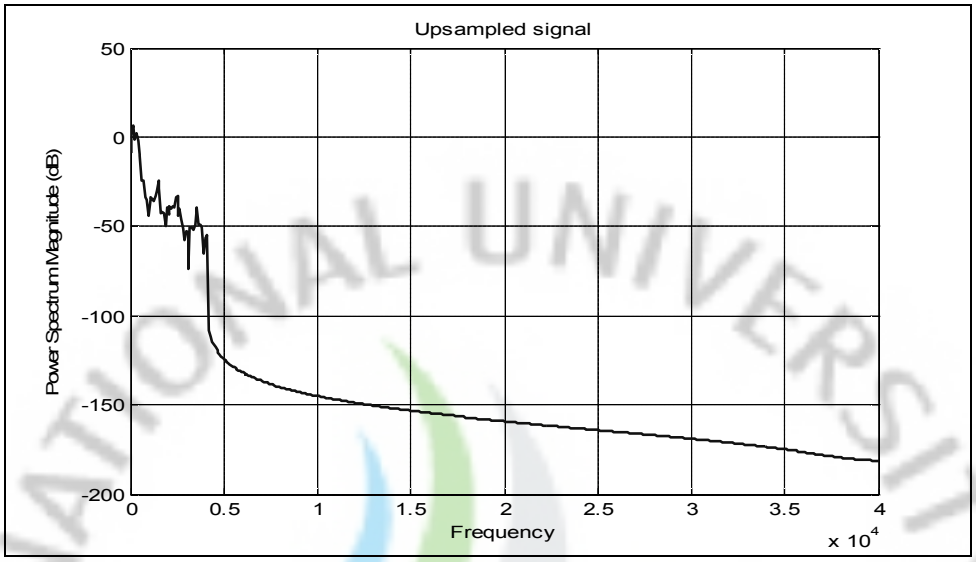

Figure 30 Upsampled audio signal

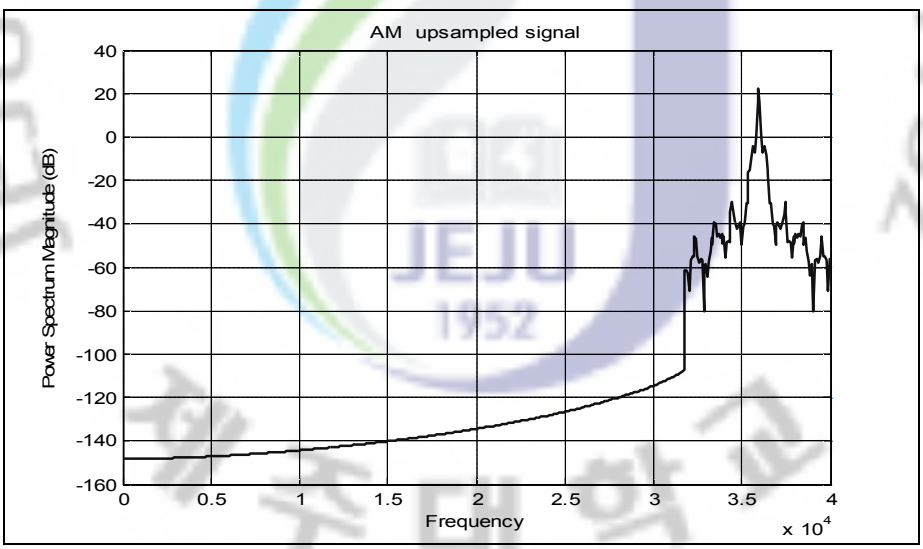

Figure 31 Amplitude modulated signal

After the upsampled AM signal is passed through the 'air channel', and the demodulated data is obtained, as seen in Fig.32, we calculate the Power spectral density (PSD) of the output data. The PSD of the output signal is low due to the high distortion levels that exist in the demodulated data.

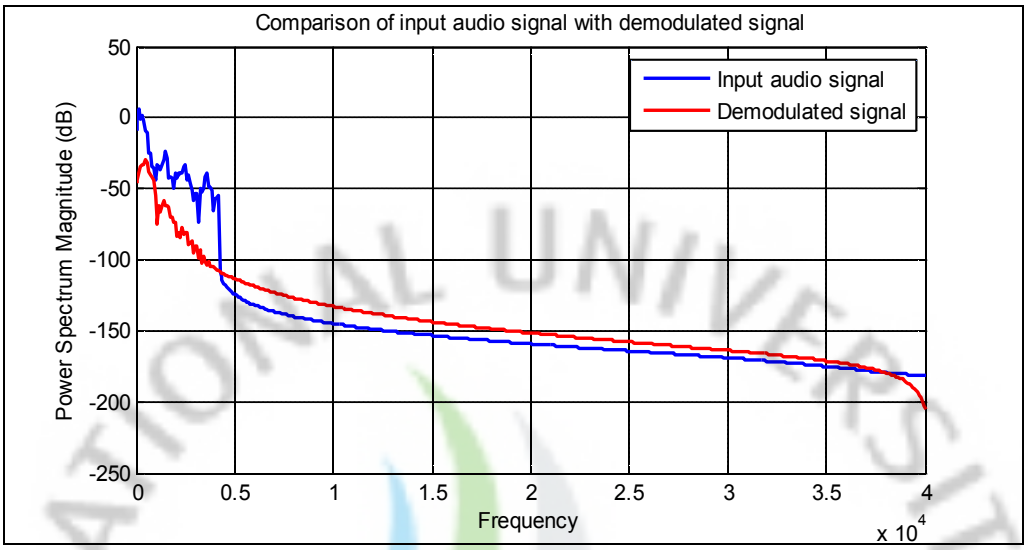

Figure 32 Demodulated data

In order to reduce the distortion, we square root the input signal before amplitude modulation. The reason behind the square root process is that, the 'air channel' is no more than a squaring process which leads to numerous harmonics which in turn results in increased distortion. Therefore to reduce this distortion, we opt to square root the input signal before it is amplitude modulated and passed to the KZK model. After the square root process, we need to make sure that the frequency components do not slip into the audible range, below 20 kHz. However if frequency components do exist in the audible range, they can be removed by passing the amplitude modulated data through a Highpass filter.

As a result of the square rooting the signal before modulation and transmission leads to a demodulated signal with lower distortion values.

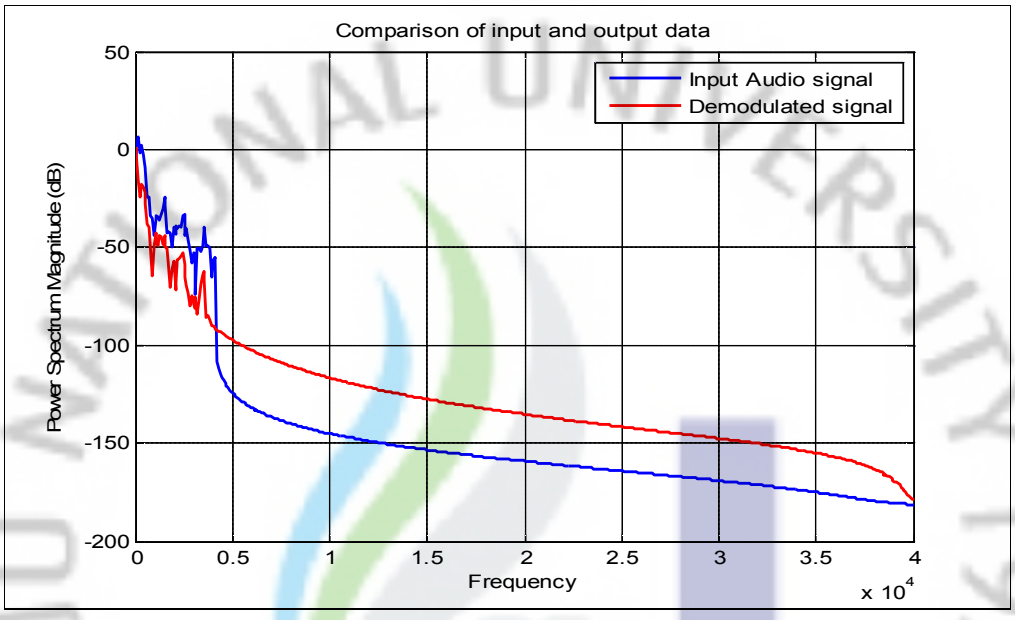

Figure 33 Comparison of demodulated data and input audio signal

From the Fig.33, it is obvious that we are able to achieve a better output by square rooting the signal before modulation.

4.2. Effect of the radius of the transducer on the output:

Consider a transducer of radius 15 cm. With a sampling frequency of 80 kHz and a carrier frequency of 35.9 kHz, we have a Rayleigh distance of 7.6 meters. As seen in an earlier section, low transducer size will not help in increased output pressure levels, which means that the demodulated signal will not be able to travel far enough. Since we have a Rayleigh distance of 7.6 meters, the desired demodulated signal can be found at 7.6 meters and higher. Once the secondary frequency is completed demodulated, we will calculate the Power spectral density as a reflection of the signal's distortion and energy level.

At a distance of 3.0 meters

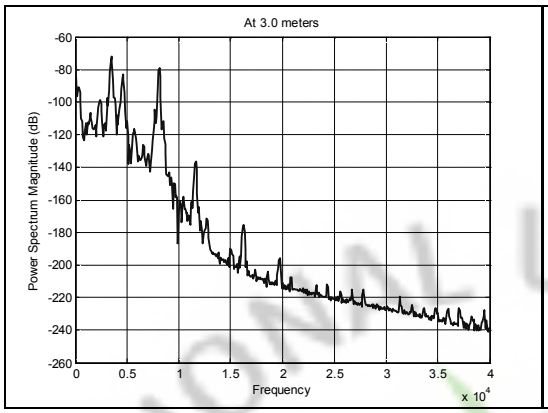

At a distance of 4.6 meters

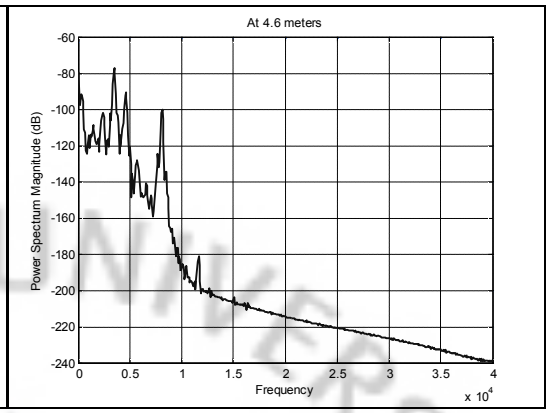

At a distance of 7.6 meters

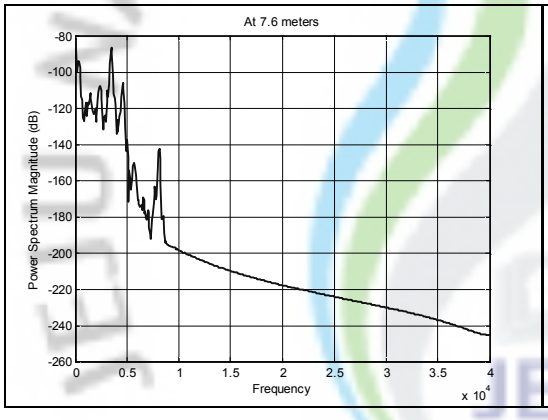

At a distance of 10.7 meters

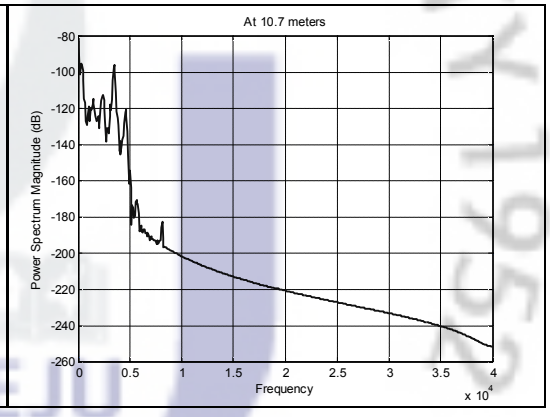

Figure 34 Demodulated output for a transducer of radius 15 cm

From the above plots, it can be seen that the demodulated wave takes shape as early as 3 meters, in the nearfield. As stated earlier, for Berktay's solution to be valid, the absorption length has to be less than the Rayleigh distance. The absorption co-efficient is 0.0202. This gives an absorption length of 49.5 meters. Therefore with a transducer of size 15 cm, and a carrier frequency of 35.9 kHz, the above demodulated output does not satisfy Berktay's demodulated output. Hence the above parameter conditions are not desirable.

Therefore let us consider the case of using a transducer of size 30 cm with a carrier frequency of 35.9 kHz. A transducer of radius 30 cm with a sampling frequency of 80 kHz and a carrier frequency of 35.9 kHz will have a Rayleigh distance of 30.7 meters. As we have a Rayleigh distance of 30.7 meters, the desired demodulated signal can be found at 30.7 meters and higher.

For Berktay's solution to be satisfied, the absorption length should be less than the Rayleigh distance. For a carrier frequency of 35.9 kHz, the absorption co-efficient is at 0.0202. Therefore we have an absorption length of 49.5 meters. Looking at the plots below,

At a distance of 15.3 meters

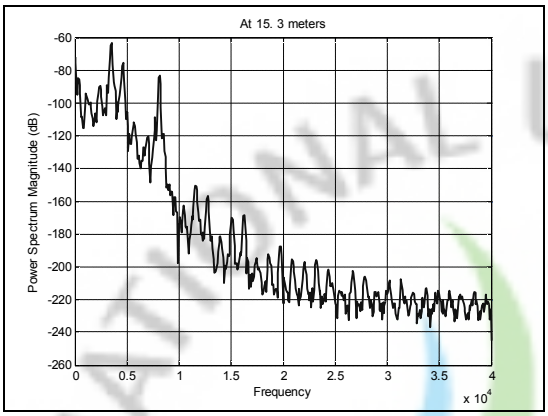

At a distance of 24.6 meters

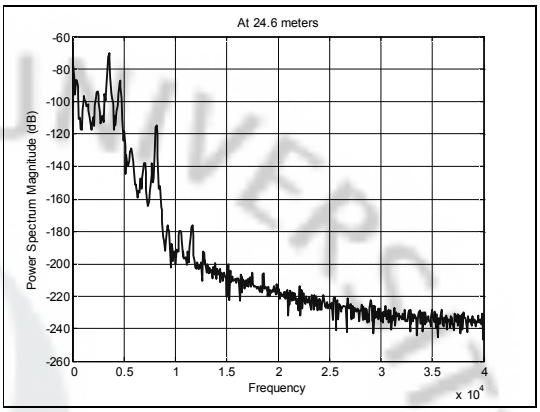

At a distance of 30.7 meters

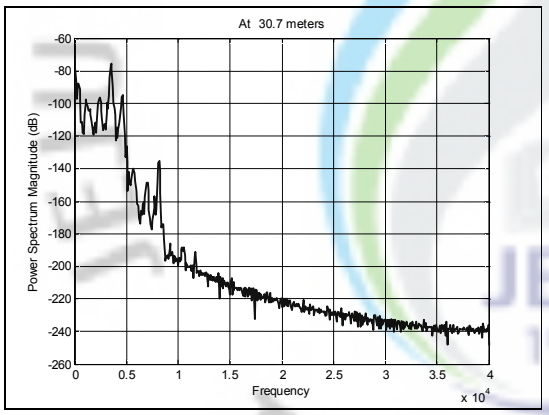

At a distance of 52.2 meters

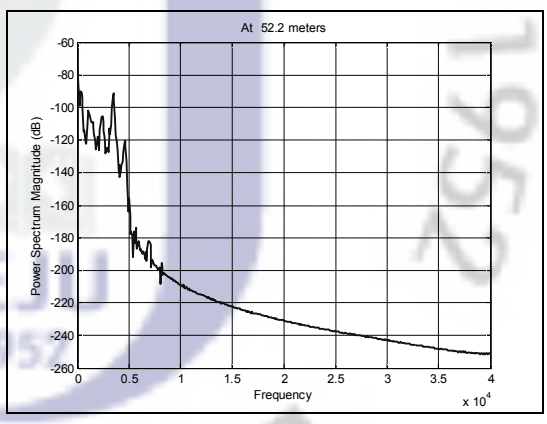

Figure 35 Demodulated output for a transducer of radius 30 cm

At the fourth plot in the above figure, the secondary frequency is almost free of additional frequency components that might cause distortion which looks good. However the Berktay's solution is still not satisfied since the absorption length remains greater than the Rayleigh distance.

Hence the ideal condition would be take a carrier frequency of 45 kHz and above with a piston of radius 30 cm. This would result in an absorption length of 31.6 meters and a Rayleigh distance of 37.09 meters and the Berktay's solution will be satisfied. It should be mentioned that since the carrier frequency is increased, the sampling frequency will have to be increased to a minimum of 100 kHz.

At a distance of 12.5 meters

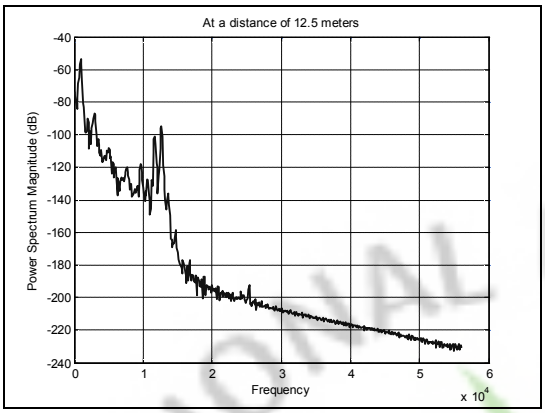

At a distance of 33.4 meters

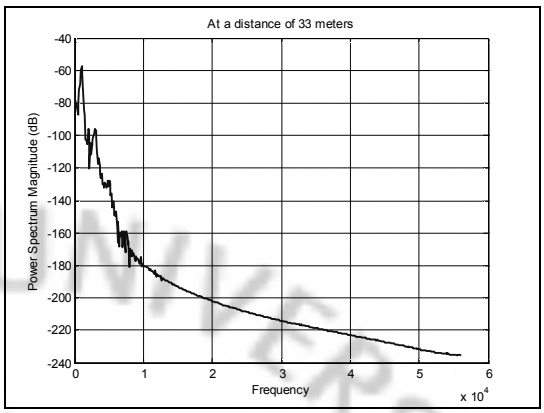

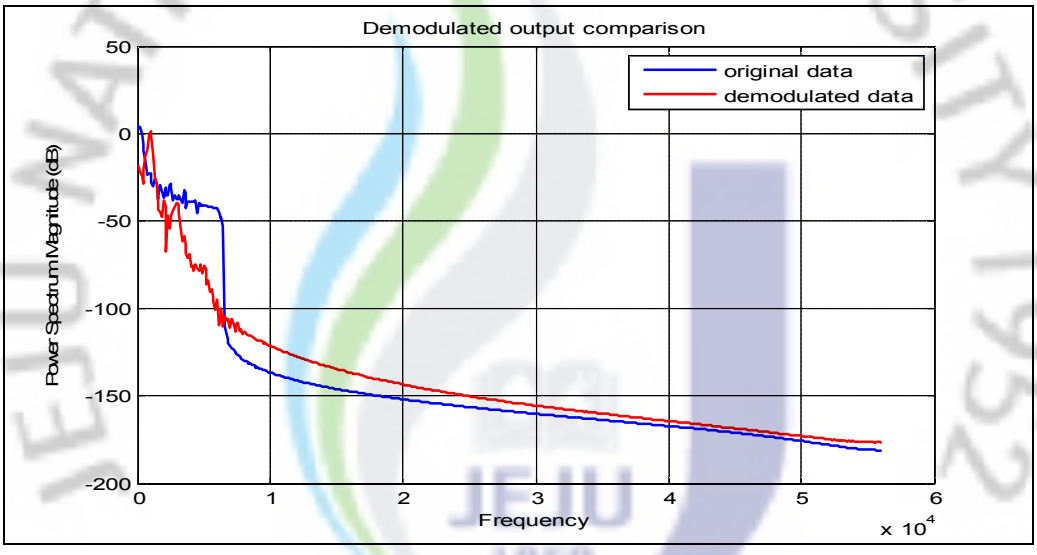

Figure 36 Demodulated data at 41.7 meters

Thus increasing the sampling frequency to a total of 112 kHz gives a carrier frequency of 49.6 kHz. We see that we have to wait for a certain distance before we lose the high frequency components that contribute towards distortion. We know that we have a f_{max} of 4 kHz. But at that distance of 41.7 meters, we see that the demodulated signal has reduced in power. Frequency components above 2 kHz are attenuated while frequency components lesser than 2 kHz are in agreement with the original signal. In order to check if this is irrespective of the sampling frequency, we take an audio signal and upsample it to 112 kHz. Therefore by upsampling, we are able to confirm that the Berktay's solution is satisfied. It should be mentioned that in the process of comparison plots, since the demodulated wave is highly attenuated, it is multiplied by an amplification factor of 100. This amplification factor is used in all comparison plots.

CHAPTER V

PREPROCESSING RESULT OF THE AUDIO SIGNAL

The two things mentioned earlier was that selecting a high frequency and applying a square root operation to the audio signal helps us overcome Total Harmonic Distortion. But as a result of the square root operation, a wide bandwidth transducer is required. In practical applications, a wide bandwidth requirement is not only a burden, but also not a feasible option. Therefore in order to overcome this disadvantage, we can opt for a Single Side Band (SSB) modulation coupled with a distortion reducing scheme [10]. Applying a SSB modulation scheme helps us overcome this bandwidth requirement while still achieving low distortion values. The simple distortion reducing scheme is as follows,

Step 1: With the audio signal, $x(t)$ as the input, we do a SSB modulation with a carrier frequency, $f_{CARRIER}$.

Step 2: The modulated signal is passed through an air channel model. The air channel can be modeled by concatenating a demodulator, a squaring function and a high pass filter followed by a gain value of unity.

Step 3: The signal obtained from step 3, the demodulated signal is compared with the original audio signal. As a result of this comparison, we obtain the difference signal, which we call the distortion signal. This distortion is multiplied with a constant, 'c' to produce $x_1(t)$. Now a negative, $-x_1(t)$ is summed with $x(t)$ to produce $x_2(t)$.

Step 4: Steps 2 and 3 can be repeated till no further improvement is obtained.

Step 5: The output obtained from step 4 can be sent into an 'actual' air channel after it is SSB modulated to obtain the demodulated output with reduced distortion.

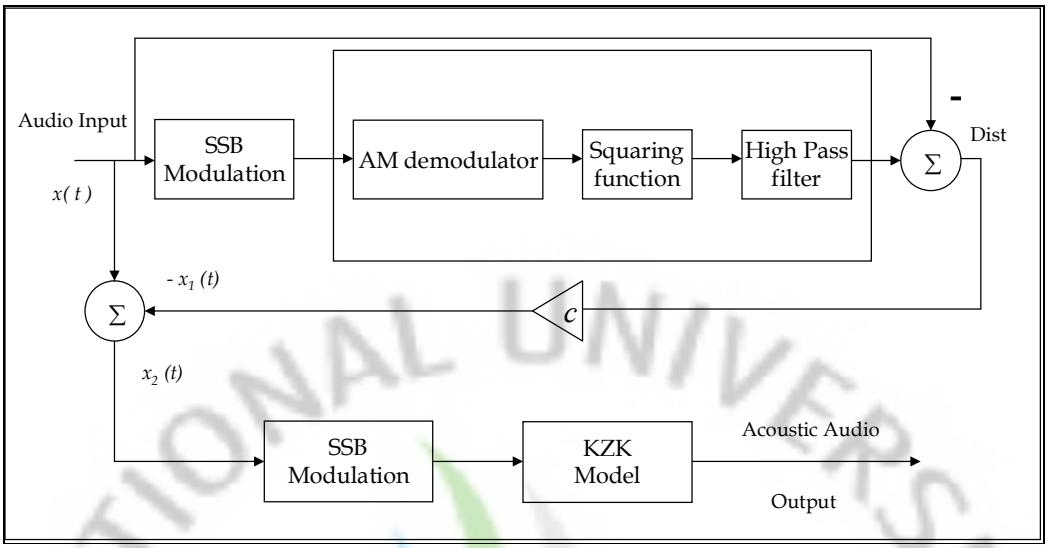

Figure 37 Layout of the parametric communication system

The SSB modulation is carried out based on the following block diagram.

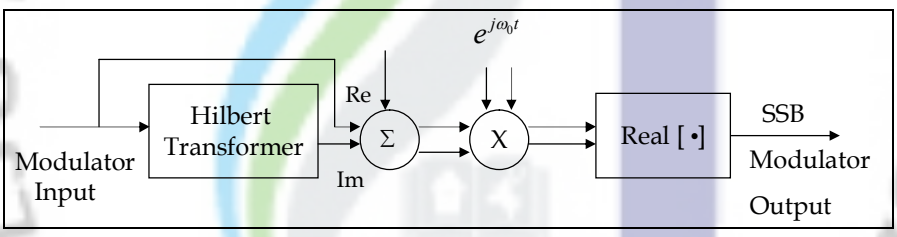

Figure 38 SSB block diagram

5.1. KZK time domain model:

For the time domain code that is used to model the propagation of a finite amplitude axisymmetric source, it is of utmost importance to select the appropriate parameters for accurate results. Given below is a table with certain parameters that were used in the time domain code.

Using the same upsampled audio signal, we use the above pre-processing scheme to obtain the demodulated data. One of the restrictions that we faced while performing the simulations was the computational cost. Due to the upsampling process, the total number of samples increases from 39922 samples to 131072 samples. Referring to the earlier mentioned KZK model, if we want a complete signal demodulation, we need to specify a time window that is larger than the input source file.

Parameters	Values used in the time domain code
ρ_{max}	10
$\Delta\rho$	1/30
$\Delta\sigma$	.001 (nearfield)
	.0035 (farfield)
$\Delta\tau$	.0261
τ_{min}	0
τ_{max}	27 (depends on the input signal length)

Table 1 KZK parameters

Taumin and Taumax values and the Delta tau values should be able to accommodate the entire length of the audio source. For example, a one-second audio sample using a 45 kHz carrier generates 45,000 (total number of cycles per second) * 60 (data points per cycle) * 1 (envelope duration) = 2,700,000 time data points per single space grid. The total data points at each range step is then calculated by multiplying this number by the number of transverse spatial data points, 60 (transverse grid size) * 12 (maximum transversal space size) = 720. Thus, the total number of data points is 1.944 *10 ^9. Various trials on different computers resulted in memory errors due to the computer not being able to support such a high computational task. Therefore we had to clip the input signal to a minimum possible number of samples to be able to still achieve a complete sinusoidal wave to override the computational demand.

As a result, we took a total of 100 samples of the audio signal. With a Delta tau value of .0261, a Taumin and Taumax value of 0 and 27 respectively, we designed a time window to accommodate the input signal. Now the input signal of 8 kHz is upsampled to a sampling frequency of 80 kHz and passed onto the SSB modulator. We employ a carrier frequency of 36 kHz.

Now we follow the distortion reducing scheme. The modulated signal is passed through the 'channel model' as explained in step 2. The output of the channel model is summed with a

negative audio signal. This results in a 'distortion component'. This distortion component is multiplied with a constant 'c', which has a value of unity. The value of 'c' can be varied between 0 and 1. The negative value of this is summed with the audio signal. As mentioned earlier, steps 2 and 3 are repeated while the distortion values are checked. Till the point of no further reduction in distortion, steps 2 and 3 can be repeated.

After step 4 is complete, we SSB modulate the signal and pass it through the KZK channel. We should ensure that we do not have any frequency components in the audible range before transmitting the signal into the KZK channel model in order to reduce distortion. In our case, this is ensured by us choosing a high sampling frequency and a high sampling rate.

5.2. Procedure:

Parameter	Value
Sample Frequency	> 105 kHz
Input source radius	30 cm
Carrier Frequency	> 45 kHz
No. of Watch points	28

Table 2 Ideal input parameters

Since we know that a transducer of radius 30 cm is desirable, we accordingly do so and do not perform simulations for a transducer of radius 15 cm. We begin the simulations with a carrier frequency of 36 kHz. The Rayleigh distance, given by Eq.8, is 7.4 meters. The modulated signal is then passed into the KZK model. The KZK model which has a total of 28 'watch points' gives the demodulated signal at various distances along the axis of the beam. The distance, in meters is given by the product of the sigma value along the axis of the beam and the Rayleigh distance. Now at a distance of 24.4 meters, the demodulated signal takes shape. But the presence of higher frequency components leads to distortion. The audio input source of 1024 samples, is as shown Fig.39.

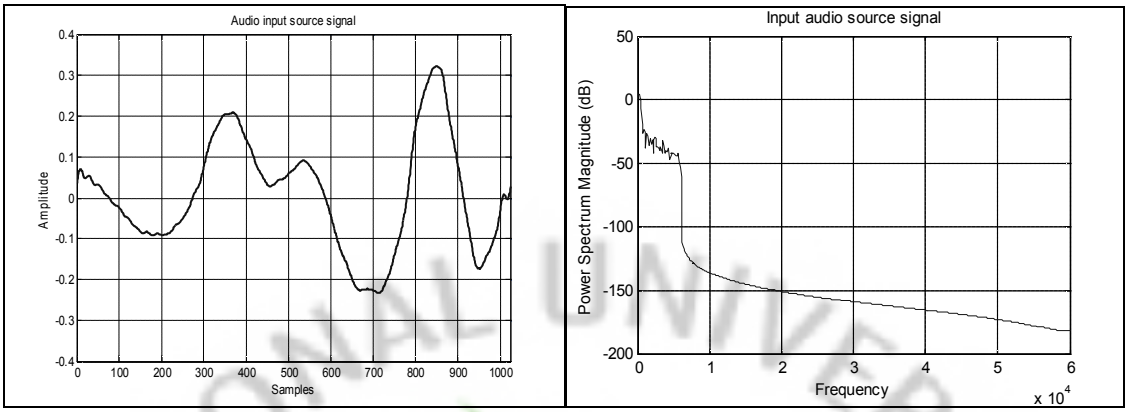

Figure 39 Audio input source signal

To observe the propagation wave, we analyze the demodulated wave at two distances as can be seen in the figure below at distances of 30.7 meters, and 52.2 meters. Since the Rayleigh distance is still lesser than the absorption length, the above plots do not satisfy the Berktay's criteria. Hence as stated earlier, the sampling frequency has to be increased to a minimum of 100 kHz to accommodate a carrier frequency of 40 kHz or higher.

At a distance of 30.7 meters

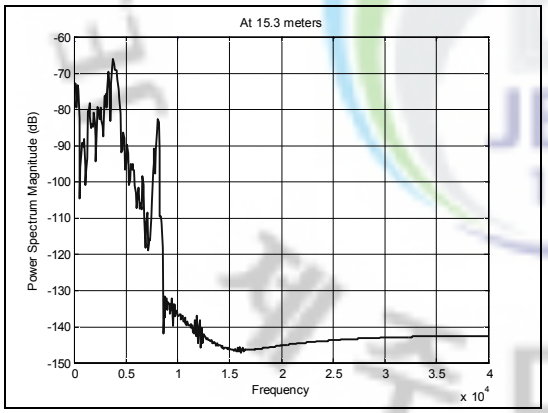

At a distance of 52.2 meters

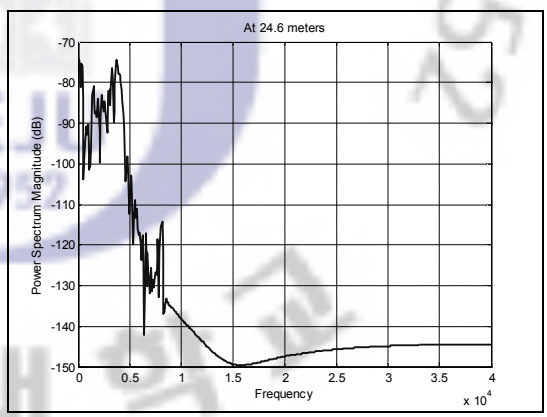

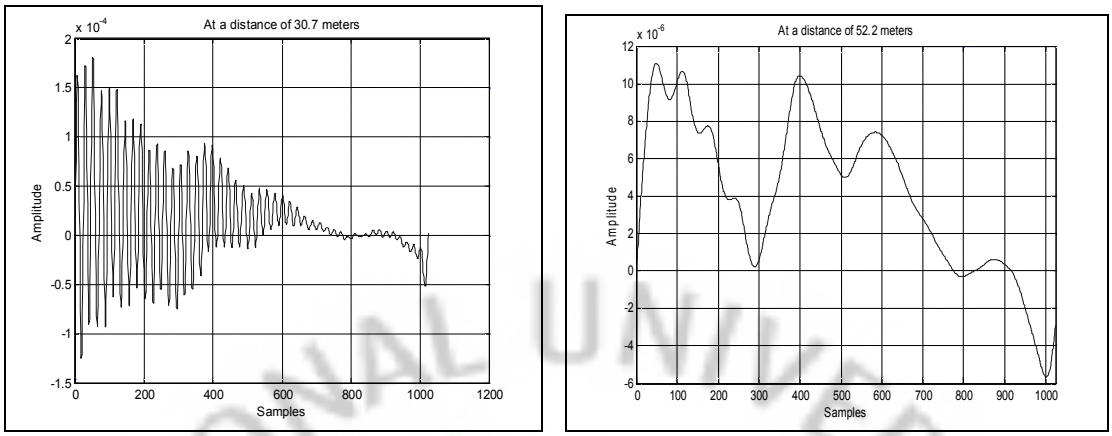

Figure 40 Demodulated data in the frequency and time domain

At a distance of 30.7 meters At a distance of 52.2 meters

Therefore the sampling frequency was raised to 112 kHz with a carrier of 49.656 kHz. The radius of the transducer was assumed to be 30 cm. The upsampled signal was passed into the SSB modulator, and then into the demodulator block. After demodulation, it was passed into the squaring block and subsequently into the high pass filter (HPF) block. The output from the HPF block was used to obtain the distortion value and this distortion signal was multiplied with a constant 'ε', 1. Further the signal was summed with the original audio signal. This was repeated for a total number of four loops.

The output at the end of four iterations was again passed into a SSB modulator block and eventually passed into the KZK model. As a result of passing the signal into the KZK channel, which substitutes as the air channel, we obtain the demodulated signal as seen in the plots below.

At a distance of 21.2 meters At a distance of 33.9 meters

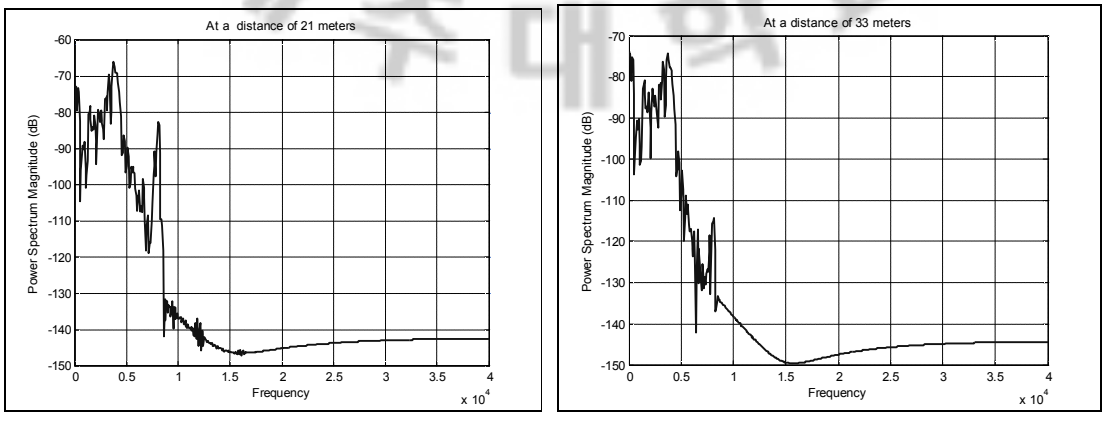

At a distance of 42.4 meters

At a distance of 50.9 meters

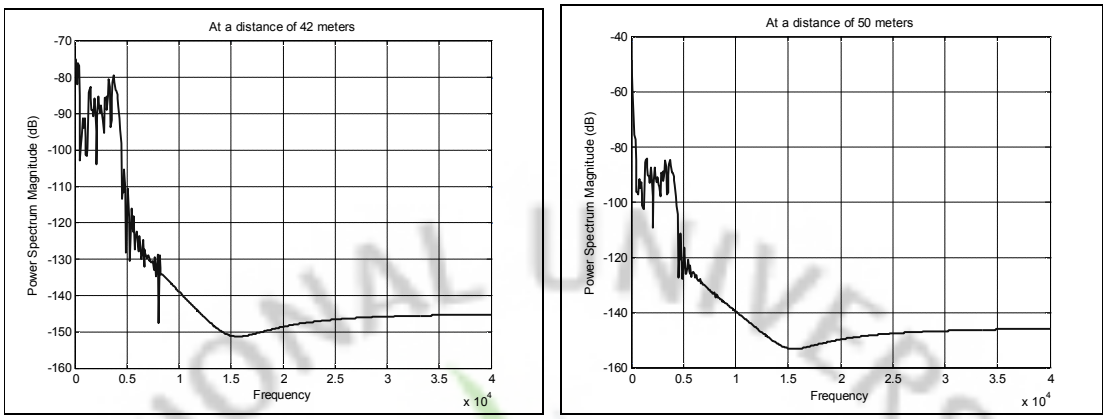

Figure 41 Demodulated data at various ranges

Therefore this gives an absorption length of 28.9 meters and a Rayleigh distance of 40.9 meters. Hence since the absorption length is smaller than the Rayleigh distance. Using the ideal parameters, we see that at the nearfield, in the first two blocks, we have additional frequency components that contribute towards distortion. However beyond 41 meters, the additional frequency components get attenuated. In the time domain, the demodulated output is as shown in Fig42. Thus abiding by the earlier rule, with these parameters, the Berktay's solution is satisfied. The demodulated output obtained is calculated for the power spectral density percentage as shown in the following section.

At a distance of 21.2 meters

At a distance of 33.9 meters

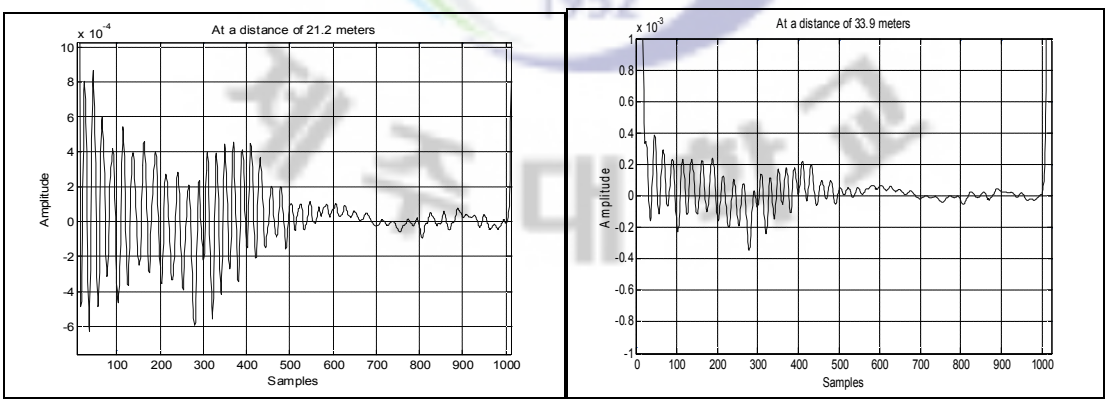

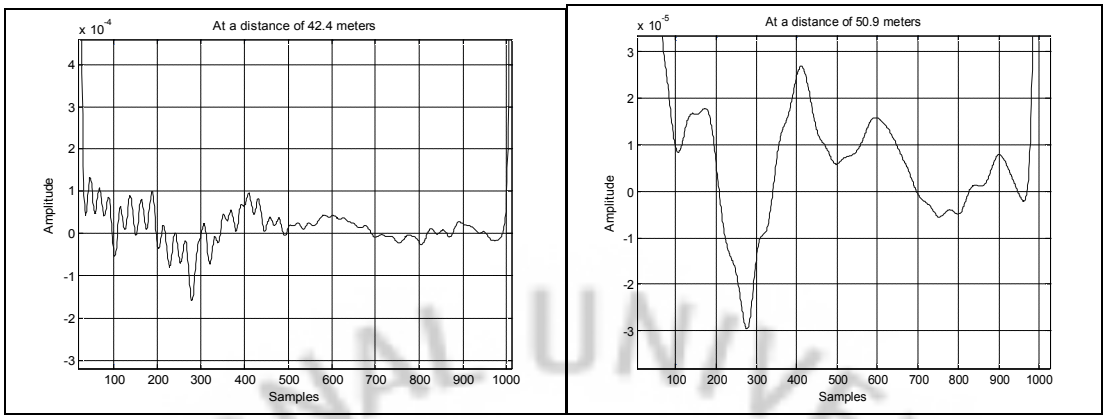

Figure 42 Demodulated output at various distances

At a distance of 42.4 meters At a distance of 50.9 meters

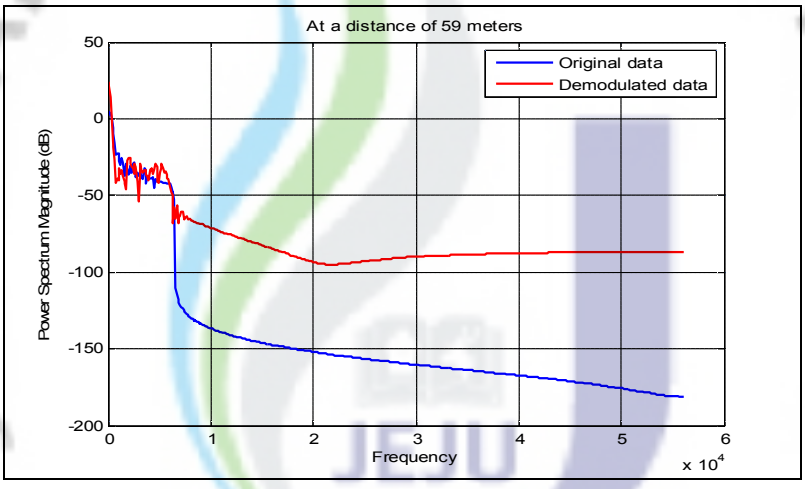

Figure 43 Comparison of demodulated signal with the original signal

5.3. Power Spectral Density:

Now we calculate the power spectral density to compute the average power in the signal, i.e. the demodulated wave. In order to be able to do so, there are two terms that are brought into consideration. The first term, is the DC component and the next is the Nyquist rate. In the mathematical form, it can be denoted by the following expression. The PSD is the Fourier transform of the autocorrelation function of the signal. This results in the formula,

$$S(f)=\int_{-\infty}^{\infty} R(\tau)\, e^{-2\pi i f \tau}\, d\tau . \qquad (31)$$

The power of the signal in a given frequency band can be calculated by integrating over positive and negative frequencies,

$$P = \int_{F_1}^{F_2} S(f)\,df + \int_{-F_2}^{-F_1} S(f)\,df. \tag{32}$$

Where, F_1 and F_2 indicate the frequency band, the DC component and half the Nyquist rate. The DC component is calculated to be at 200 Hz. The Nyquist frequency is half the sampling frequency. Since the sampling frequency is 112 kHz, half the Nyquist rate would be 56 kHz.

As a reflection of the distortion inherent within the signal, we calculate the power spectral density of each demodulated wave and compare it against the input signal. The resultant percentage value is computed for the different modulation methods employed. Once the PSD of the demodulated signal is calculated, it is compared with the PSD of the original signal to compute the percentage. The difference in percentage among the different demodulated signals can be seen in the table below. During computation of the power spectral density, no amplification factor was used. The Power spectral density function (PSD) thus shows the strength of the energy as a function of frequency.

Preprocessing Methods	Power Spectral Density percentage
AM signal with no square root	.2 %
Square rooted AM signal	23 %
SSB signal with preprocessing	21%

Table 3 Power spectral density percentage

In order to have a dependable output, we use only the signal portion of the demodulated signal to obtain the Fourier transform. The input signal has a total of 1024 samples. It has been mentioned in the earlier chapter that during the KZK process, we need to ensure that a 'time window' larger than the signal is maintained. Therefore at the output, care is taken to ensure that we take the Fourier transform of only the signal and not the zero values that might occur at the output. Therefore the Fourier transform of the demodulated signal is also only for 1024 samples of the output signal.

Based on the preprocessing schemes employed, the power spectral density percentage was calculated for the different input signals used. The power spectral density can be calculated using MATLAB [15]. The table above gives a clear picture of why the pre-processing scheme is effective to obtain better output while not compromising on the transducer bandwidth. Although the pre-processing scheme shows a lesser value, it is desirable due to its transducer bandwidth requirement.

Using the SSB based pre-processing scheme not only helps in maintaining the distortion levels to a minimum, it also maintains a finite bandwidth requirement. Choosing the appropriate KZK parameters and input frequency values helps us get an accurate representation of the difference frequency at a certain distance.

CHAPTER VI

BEAMFORMING AND BEAMSTEERING

Now that we know that we have a highly directional pattern in parametric array, it is only desirable that we are able to steer it in the desired direction. One of the advantages of parametric array is that we can get an almost sidelobe free beam pattern at the far field pattern along the axis of the beam. But as the beam is steered, then there is a possibility that the ratio between the main lobe magnitude and the side lobe magnitude tends to reduce due to the fact that the energy in the main lobe tends to move towards the sidelobes. Therefore care needs to be taken that while we maintain the main lobe intensity, we are able to steer the beam in the intended direction. Generally, in narrow-band systems, a "phase shift" is used to steer the array of antennas in the direction intended. This is called a phased array. But here since we deal with a broadband 'audio' signal, we prefer using the time delays, coupled with chebyshev weights, to steer the beam along the desired direction.

6.1. Beam theory:

With an arbitrary source condition, the far field response is given by Huygens principle. A very general principle applying to all forms of wave motion states that every point on the instantaneous position of an advancing phase front (wave front) may be regarded as a source of secondary spherical wavelets. The position of the phase front a moment later is then determined as the envelope of all the secondary wavelets. This principle, stated by Dutch physicist Christian Huygens (1629-95), is extremely useful in understanding effects due to refraction, reflection, diffraction, and scattering of all types of radiation, including sonic radiation as well as electromagnetic radiation and applying even to ocean-wave propagation. Huygen stated that the wavefront of a propagating wave of light at any instant conforms to the envelope of spherical wavelets emanating from every point on the wavefront at the prior instant. Huygen's principle states that any wave producing source can be modeled as an infinite number of individual sources distributed identical to the original source. A pulsating simple source radiates energy in spherical waves as given by,

$$p_{point}(R) = \frac{dp_0}{R} e^{j(wt - kR)} \tag{33}$$

where dp_0 is the source amplitude, R is the distance from the source to the point of interest, ω is the driving frequency, k is the wave number and j is a unit imaginary number.

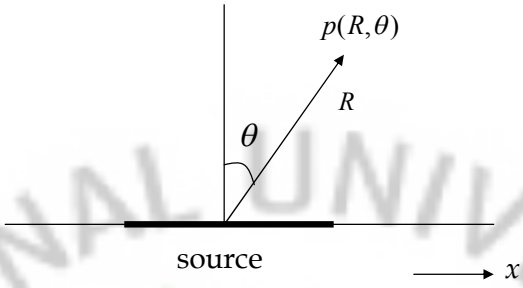

Figure 44 Geometry of source

Beam steering can be said in simple terms as 'changing the direction of the main lobe of a radiation pattern'. Therefore it is our desire to do the same for the parametric array. But as stated earlier, as the beam is steered along a direction , energy from the main beam gets dispersed to the sidelobes, so while we steer the beam we also make sure that the side lobes are attenuated in order to preserve the directionality of the parametric array.

6.2. Beamforming for a parametric speaker:

All analyses in the following section are based on the KZK wave equation. Let us assume that the source has a radius 'a'. With the Rayleigh distance in consideration, substituting the Green's function in Eq.6, results in,

$$q_1(\theta,z) = jkz^{-1}\, e^{-\alpha_1 z}\tilde{q}_1(k\tan\theta,0)\exp\left(-\frac{1}{2}\, jkz\tan^2\theta\right) \tag{34}$$

Where, θ is the angle with respect to the axis of the beam. Now the farfield solution from the above equation leads to,

$$D_1(\theta) = \exp\left[-\frac{1}{4}(ka)^2\tan^2\theta\right] \tag{35}$$

Larger values of *ka* lead to narrower beams and the farfield directivity of the parametric array is $D_{1a}(\theta)D_{1b}(\theta)$. There are different kinds of beamformers that can be used for this application, however we prefer to use the delay and sum beamformer. With an assumption of M elements arranged in a uniform linear array with an interelement spacing of *d* meters, we design the beam

pattern of the parametric array . After the beam pattern is designed, we steer the beam at a direction θ as desired.

The array response for the delay and sum beamformer is given by,

$$H(\omega\tau)=\frac{1}{M}\sum_{m=0}^{M-1} w_m e^{jm\omega\tau} \tag{36}$$

Where, $\tau=(d/c)\sin\theta$ is the time delay due to array geometry. If we desire to steer the beam at an angle, θ_0, a time delay of $m\tau_0$ has to be added to the m^{th} transducer before the transmission of the parametric array[7]. Now the difference frequency's farfield directivity is given by the product of the array response and the farfield solution from Eq.33,

$$D_{-}(\theta) = D_1(k_a,\theta)H(k_a,\theta)D_{1b}(k_b,\theta)H(k_b,\theta) \tag{37}$$

From an earlier section, we see that in order to maintain low distortion levels while still using a nominal transducer bandwidth; we employ a Single Sideband modulation scheme. Therefore the output of the Single Sideband modulator is given as,

$$\varphi_{SSB}(t)=0.5m\cos(\omega_{-}t)\cos(\omega_c t)\pm 0.5m\ \sin(\omega_{-}t)\sin(\omega_c t) \tag{38}$$

In order to reduce distortion, we maintain that we do not let the audible frequency slip into the audible range. To ensure this, we take only the upper side band of the modulated signal before it is passed onto the KZK model. In accordance with this, the modulated output signal for USB with carrier is

$$\varphi_{USB-WC}(t)=0.5\{\cos(\omega_c t)\}+m\cos\left[(\omega_c+\omega_{-})t\right] \tag{39}$$

Since sidelobes are not prominent in parametric array, we do not emphasize on the aspect of sidelobe reduction. However we still calculate weight values to suppress any sidelobes that might arise out of the steering process. The weight values are calculated based on Chebyshev weighting functions.

The weighting function w_{am} is calculated based on a chebyshev weighting function. In order to calculate the chebyshev weighting function, we specify the sidelobe attenuation level, R and the number of ultrasonic transducer array, M. R is calculated based on the formula,

$$R = 20 \log \left\{ T_{2N} \left[\frac{\cos\left(\frac{\pi}{2(M-1)} \right)}{\cos\left(\frac{k_a d \sin(\theta_- / 2)}{2} \right)} \right] \right\} \tag{40}$$

Where,

$T_{2N}(x) = \cos\left[(M-1) \cos^{-1} x \right]$ is the chebyshev polynomial

θ_- = difference frequency

After the value of R is determined, we obtain the first set of weight values in w_{am}. Using the values of w_{am}, employ the formula,

$$H(k_a, \theta) = \frac{1}{M} \sum_{m=0}^{M-1} w_{am} e^{jm\omega(\sin\theta * d / c)} \tag{41}$$

From Eq.41, we calculate the peak of the first side lobe to determine, θ_{peak}. We further use the same Eq.41 to calculate $H(k_b, \theta)$ with $\theta_- = \theta_b$ and $k_a = k_b$. With a carrier frequency of 36 kHz, an inter-element distance of 4.9mm, a source radius of .15 m and a total of 16 elements for the linear array, there are two weighting functions w_{am} and w_{bm} that are calculated. The value of *c* is 344 m/s. Initially, we specify the beamwidth required for the difference frequency. We take this to be 30 degree. With the parameters specified above, using Eq.40 we obtain the sidelobe attenuation level, R.

m	w_a	w_b
1	0.2671	0.0005
2	0.3046	0.0052
3	0.4435	0.0288
4	0.5915	0.1029
5	0.7350	0.2653
6	0.8595	0.5217
7	0.9513	0.8071
8	1.0000	1.0000

Table 4 Weight Values

With the value of R obtained, the w_{am} weight values are calculated. Now using this weight value and the Eq.41, we plot the array response function. As mentioned earlier, sidelobe reduction is not much of a concern in parametric array due to its high directivity. In spite of which the location of the first sidelobe is calculated to obtain w_{bm} weight values. Once the weight values are obtained, the farfield directivity is plotted as can be seen in the figure below.

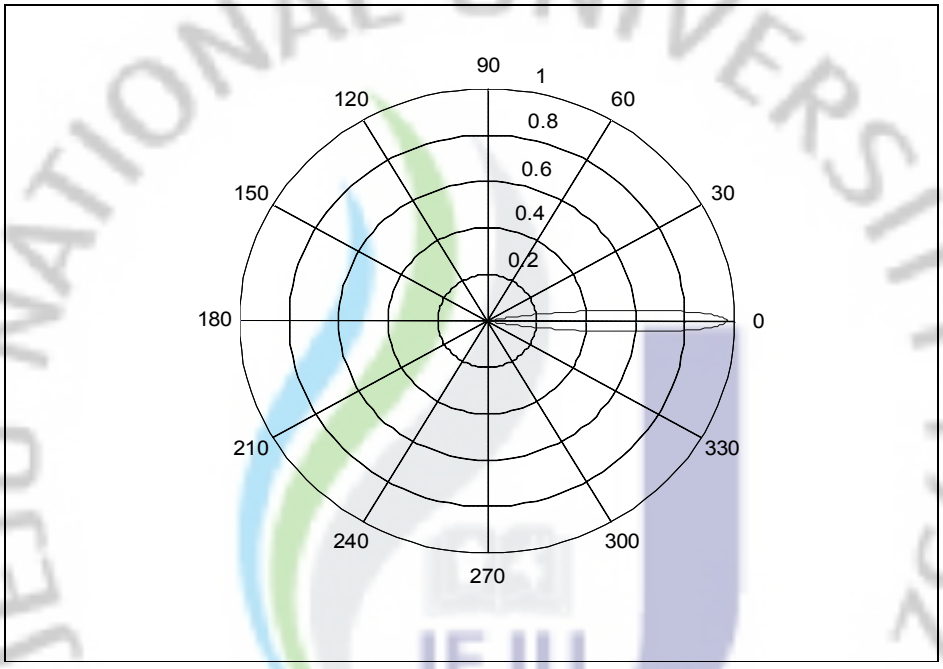

Figure 45 Difference frequency directivity

In order to be able to steer the beam in the desired direction, we use time delays.

The time delays are given by, $\tau_0 = (d/c)\sin\theta_0$. Substituting the time delay in Eq.41, gives,

$$H(k_a,\theta) = \frac{1}{M}\sum_{m=0}^{M-1} w_{am} e^{jm\omega((\sin\theta_0 - \sin\theta)*d/c)} \tag{42}$$

The steering angle considered was 20^o. As mentioned earlier, sidelobe reduction is not to be bothered with, due to parametric array's high directivity. But during the process of steering, energy from the main lobe is transferred to the side lobes. Therefore care should be taken that the side lobes are reduced in order to be able to concentrate all the energy in the desired direction, in this case 20 degrees. Hence the array response function is calculated using Eq.42. From the array

response calculated, the peak location of the first sidelobe is determined which helps in obtaining w_{bm}.

$$H\left(k_b,\theta\right)=\frac{1}{M}\sum_{m=0}^{M-1}w_{bm}e^{jm\omega((\sin\theta_0-\sin\theta)*d/c)} \tag{43}$$

After the weight value of w_{am} and w_{bm} are obtained, as can be seen in table 4, we calculate difference frequency far field directivity based on the Eq.37 for a steering angle of 20^o.

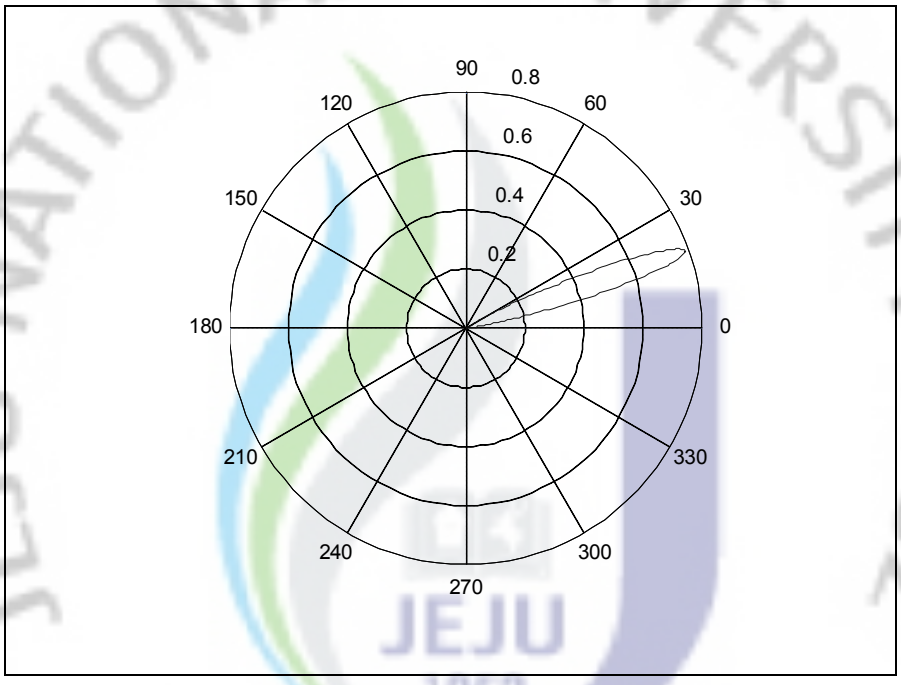

Figure 46 Difference frequency directivity steered to an angle of 20 degrees

The directivity of the parametric array is dependent on the absorption length of the signal and the Rayleigh distance. Since the ratio of the Rayleigh distance to the absorption length determines the length of the non-linear interaction region, the input primary frequency and the diameter of the audio source are of utmost importance to be able to obtain a high directive signal at the output. It is evident from the figure that there is a reduction in power when the beam is steered away from the axis. Some of this energy lost is due to the energy being spilled onto the sidelobes from the main lobe. Therefore in the beamforming algorithm, the weight values are designed in such a way that the side lobe is suppressed while steering the beam in order to be able to maximize the main output.

Using the same quasilinear approximation of the parametric array, it can be shown that the half power directivity, which is the angle between the points in the main lobe where the amplitude has dropped by 3 dB, is,

$$\theta_{HP} = \sqrt{\frac{2\alpha_T}{k_D}} \tag{44}$$

Where,

$\alpha_T = \alpha_1 + \alpha_2 - \alpha_D$ with α_1 , α_2 and α_D being the absorption co-efficients at the frequencies F_1, F_2 and F_d and k_D is the wave number of the difference frequency.

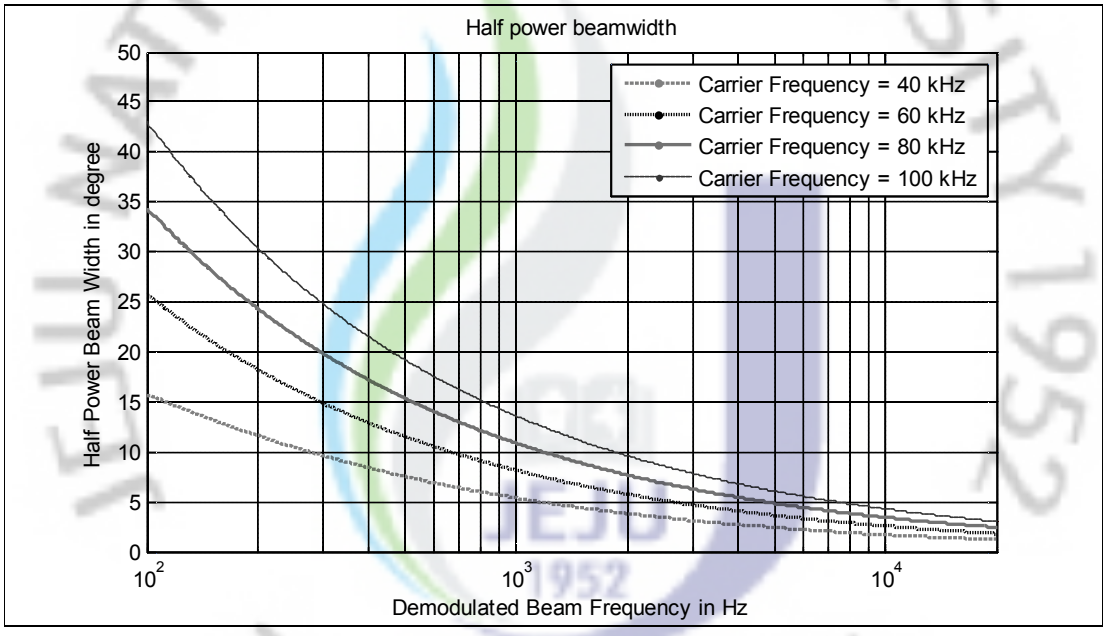

Figure 47 Half power beamwidth

The above plot justifies what has been said in the previous chapters. High carrier frequencies have high values of half power beamwidth, therefore low value of carrier frequencies are not ideal.

The demodulated pressure along the axis is given by Berktay's solution. In section x, we looked at the different parameters that help us achieve an accurate representation of the demodulated signal. Now in order to see the relation between the radiuses of the piston and the demodulated pressure along the axis we take a look at Berktay's equation once again. It is given by,

$$p_2(0,z,t') = \frac{\beta p_o^2 a^2}{16\alpha_0 \rho_0 c_0^4 z} \frac{d^2 E^2}{dt'^2} \tag{45}$$

Where,

β = co-efficient of nonlinearity

p_0 = amplitude of the primary carrier frequency

a = source radius

α_0 = attenuation co-efficient

ρ_0 = density of the propagation medium

z = axial distance from the source and

c_0 = speed of sound in air and

E = envelope function.

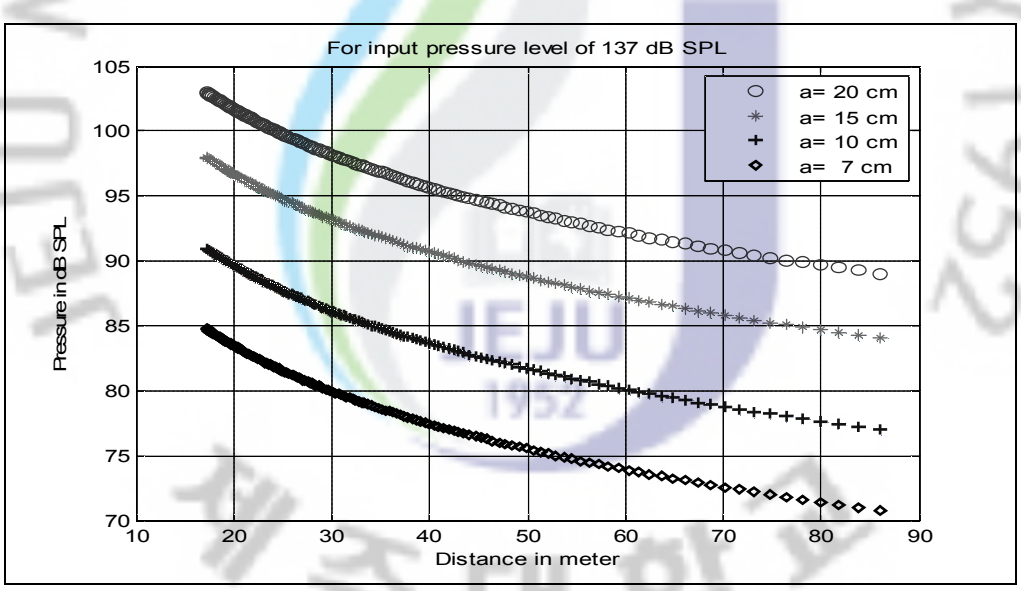

Figure 48 Output pressure level

As mentioned earlier, increasing the piston size helps in obtaining higher output pressure levels without causing saturation. The pressure value naturally reduces with increasing distance. Some of the values taken here to compute the Sound Pressure Level are,

$$\beta = 1.2$$

$\rho_0 = 1.21\ \text{kg} / \text{m}^3$
a = 15 cm.
c = 343 m/s.
$\alpha_0 = 0.0202$ and
z = 10 – 90 meters.

In spite of the fact that a practical experiment was not carried out to confirm the results of the numerical simulation, a limitation of parametric array, the biological effect that surrounds the ultrasound carrier frequency involved is acknowledged. Future work involved can be based on nullifying this effect. Another area of improvement in the numerical code is to be able to reduce the computation time without compromising on the accuracy of the result.

CHAPTER 7

CONCLUSION

With the help of the time domain code, we show that using a square root option before the signal is modulated, helps reduce distortion. However due to the infinite bandwidth requirement, we opt for a SSB based pre-processing method to show that we can improve the distortion while still maintaining the bandwidth levels of the transducer to a practical and feasible limit. We performed simulations based on the different radiuses that the transducer can use and concluded that a radius of 30 cm coupled with a primary carrier frequency of 49 kHz and above remains ideal parameters while using the KZK model to design a parametric array setup. Should one wish to reduce the size of the radius of the piston to below 30 cm, then the primary carrier frequency needs to be increased to make sure that the absorption length remains lower than the Rayleigh distance. With the help of recursive trials, we also find the optimum values for the KZK time domain code in order to get an accurate audible response at the output while maintaining the computational load. A beamforming algorithm was also implemented to steer the demodulated beam in the desired direction and the half power beamwidth for the demodulated signal along the axis of the beam was plotted.

REFERENCES

Periodicals

[1] Peter J. Westervelt, "Parametric Acoustic Array", J.Acoust.Soc.Am. Vol 35, No 4, April 1963.

[2] Masahide Yoneyama and Jun-ichiroh Fujimoto, "The audio spotlight: An application of nonlinear interaction of sound waves to a new type of loudspeaker design". J.Acoust.Soc.Am, Vol 73, No 5, May 1983.

[3] Jacqueline Naze Tjotta and Sigva Tjotta, "Propagation and interaction of two collinear finite amplitude sound beams". J.Acoust.Soc.Am, Vol 88, No 6, May 1990.

[4] H.O. Berktay, "Possible Exploitation of Non-Linear Acoustics in Underwater Transmitting applications". J.Sound Vib. 2 (4): 435-461 (1965).

[5] Mary Bennett and Dr.Blackstock, Parametric Array in Air, J.Acoust.Soc.Am. Vol 57, No 3, pp 562-568, 1975.

[6] Thomas D. Kite, John T. Post, Mark F. Hamilton, "Parametric Array in Air: Distortion Reduction by pre-processing". ICA/ASA Proceedings, Seattle, WA, June 1998.

[7] Jun Yang, Woon-seng Gan, Khim-Sia Tan, Meng-Hwa Er, "Acoustic beamforming of a parametric speaker comprising ultrasonic transducers", Sensors and actuators, A 125, 2005, pp 91-99.

Books

[8] Mark F. Hamilton and David T. Blackstock, "Non-linear Acoustics", Academic press, Chestnut Hill, MA. 1998, pp 233-259.

Articles from Conference proceedings

[9] Laura A. Brooks, Anthony C. Zandler, Colin H. Hansen. “Investigation into the feasibility of using a Parametric Array control source in an Active Noise Control System”. Proceedings of ACOUSTICS 2005, Nov 2005, AUS.

Patents

[10] Michael E. Spencer, James J. Croft, Joseph O. Norris. “Modulator processing for a parametric speaker system. Patent No: US 7,162,042 B2. Jan 9, 2007.

Technical reports

[11] F. Joseph Pompei. “Sound from Ultrasound: The parametric array as an audible sound source”. PhD dissertation, MIT, June 2002.

[12] Y.S.Lee, “Numerical simulation of the KZK equation for pulsed finite amplitude sound beams in Thermoviscous fluids”. PhD dissertation, The University of Texas at Austin, December 1993.

Web links

[13] http://en.wikipedia.org/wiki/Parametric_array

[14] http://en.wikipedia.org/wiki/Beamforming

[15] http://www.mathworks.com/access/helpdesk/help/toolbox/signal/index.html?/access/helpdesk/help/toolbox/signal/dspdata.psd.html

요 약 문

본 연구에서는 음성신호에 대한 파라메트릭 배열에 관한 연구를 수행하였다. 음성신호에 대한 파라메트릭 배열은 수치모델로 해석될 수 있고 여기서 사용된 음성 파라메트릭 배열의 수치모델은 KZK(Khokhlov-Zabolotskaya-Kuznetsov). 비선형

KZK수치모델은 시간영역의 차분방정식 알고리즘을 사용하여 파라메트릭배열 응답 특성의 정확도를 높인다. 시간영역기반의 KZK모델은 음원의 크기와 전송주파수의 영향을 받으며, 가청신호응답은 출력레벨과 빔폭의 크기를 포함한다. 음성신호에 대하여 파라메트릭 배열을 효율적으로 적용시키기 위해서는 응답신호의 왜곡에 대한 고려가 중요하다. 특히 복조신호에서 왜곡이 적고 높은 출력을 갖는 최적의 파라미터를 찾는 것이 중요하다. 따라서 본 연구에서는 복조신호응답의 왜곡을 줄이기 위하여 전처리 기법을 제안하였다. 제안된 기법은 수치해석을 통해 증명되었고, 이를 이용하여 가청 신호 응답에 대한 빔패턴을 조정하였다.

ACKNOWLEDGEMENTS

I would like to thank my Professor Lee Chong Hyun for helping me through every step of my way during my two year study. I whole heartedly would like to acknowledge his guidance and help in completing this thesis. I would also like to thank all the other professors in my department for helping me in one way or another throughout the duration of the course. I would also like to thank my parents for all their prayers, love, support and affection that sustained me through. If not for my colleagues and friends whom I shared my lab and life with, I would not have seen myself through. I would also like to thank The Cheju National University for providing me the opportunity to pursue my Masters degree. I am indebted to the Korean government for providing me a scholarship to complete my Degree for which I am immensely grateful. I would finally like to thank every one of you who helped me along.